Response to Anonymous Referee #1

Understanding the relative importance of sulfate formation pathways is essential for mitigation of haze pollution in China. However, there are a lot of debates on this topic. This manuscript presents a very comprehensive examination of aerosol pH and the relative importance of sulfate formation pathways during winter haze in the North China Plain. The results elucidate the dynamic changes in both pH and chemical regimes of sulfate formation. The scientific importance and presentation are of high quality, but some details need to be added before being published. The specific comments are listed below:

We thank the reviewer for the very valuable and constructive comments, which help us to improve the study and manuscript. Please find our point-by-point response (black) and the corresponding revisions (blue and *Italic*) below.

1. Page 4, line 1: in the North China Plain

Response:

Thanks. We have revised it accordingly:

"regimes for sulfate formation may indeed co-exist in the North China Plain"

2. Page 4, line 18: Sulfate is used in other places, use sulfurous instead of sulphurous to keep consistent.

Response:

Thanks. We have replaced the "sulphurous" by the "sulfurous" throughout the manuscript.

3. Page 5, lines 5-8: This is heterogeneous uptake of NO2 on surface of fine particles, not aqueous phase chemistry. Is there any reason to include it? The purpose is not clear.

Response:

Thanks for pointing out this issue. In this study, we focus on the aerosol pH as well as detailed mechanisms for the sulfate formation (the relevant reactions rates highly depend on aerosol pH) in aerosol water. In order to better predict aerosol pH, it is necessary to reproduce the observed aerosol loadings for sulfate, nitrate and other components. And we have tested that if the heterogeneous formation of nitrate was ignored, nitrate concentrations would be underestimated. Considering that the explicit mechanisms for the aqueous phase production of nitrate are very complicated (Herrmann et al., 1999;Herrmann et al., 2005), and beyond the scope of our current study, we have adopted a parameterization scheme to simulate the heterogeneous formation of nitrate (Zheng et al., 2015;Chen et al., 2016). We have clarified this issue in the third paragraph of Section 2.2 in the revised manuscript:

"The CTRL scenario is expected to reproduce the observed fine particle compositions (including sulfate, nitrate, ammonium, chloride and crustal components) and gas phase pollutants, and thus more reliably predict the spatio-temporal distribution of pH, AWC and sulfate production."

4. Page 7, lines 14-17: Is there any observation of dissolved FE3+ or MN2+ to adjust FSFE3+ and FSMN2+. In Wang et al. (2016), observations of Fe and Mn are provided. It is not very convincing to adjust FSFE3+ and FSMN2+ based on sulfate observation here.
https://www.pnas.org/content/113/48/13630

Response:

Very good suggestion, thanks. Soluble Fe/Mn concentrations are often measured and reported in studies focusing on dust events (e.g., Takahashi et al., 2011;Shi et al., 2012;Schroth et al., 2009;Ravelo-Perez et

al., 2016). However, during the urban haze episodes, the concentrations as well as sources for Fe/Mn ions in aerosol water remain not well constrained and understood, although the observed concentrations of total Fe/Mn elements in urban $PM_{2.5}$ have been reported in some previous studies (e.g., Sun et al., 2006;Wang et al., 2006;Chen et al., 2017). Validation of the simulated Fe^{3+}/Mn^{2+} ions in aerosol water is indeed limited by the lack of observations in our study. Nonetheless, we have compared the simulated soluble Fe/Mn concentrations with the observed data reported in Wang et al. (2016). As shown in Table R1, the simulated concentrations for Fe^{3+}/Mn^{2+} at the Beijing TSU site and the Yan'an city are at the same or similar order of magnitude as the observations at a Xi'an urban site (note that the Xi'an site is outside of our simulated domain, and inside the simulated domain, Yan'an city is the nearest city to Xi'an).

Table R1. Comparison of the soluble Fe/Mn concentrations in aerosol water

	This study	This study	Wang et al. (2016)
Time	January 2013	January 2013	November-December 2012
Site location	Beijing	Yan'an	Xi'an
Soluble Fe (ng/m^3)	/	/	1.5-16
Soluble Mn (ng/m^3)	/	/	10-41
Fe^{3+} (ng/m^3)	3.2	0.6	/
Mn^{2+} (ng/m^3)	3.6	3.3	/

In this study, we have adopted 7% and 40% for FS_{FE3+} and FS_{MN2+}, respectively. The observed values for FS_{FE} and FS_{MN} both show a large variability (1-10% and 20-60%, respectively), depending on dust mineralogy and atmospheric aging (Journet et al., 2008;Schroth et al., 2009;Johnson et al., 2010;Shi et al., 2012;Claquin et al., 1999;Meskhidze et al., 2003;Takahashi et al., 2011;Duvall et al., 2008;Baker et al., 2006;Hsu et al., 2010). Our adopted values are within these ranges. We have also investigated the potential changes in predicted aerosol pH and sulfate production relevant with the uncertainties in TMI concentrations. Sensitivity tests indicate that sulfate formation is rather sensitive to the availability of TMI species, and TMI concentrations need to be better constrained in future observational and modeling studies. We have further clarified this issue in the third paragraph of the Discussion Section:

"Our results indicate that sulfate production is rather sensitive to the availability of TMI species. Unfortunately, the concentrations as well as sources for TMI species in aerosol water during haze episodes remain not well constrained and understood. The simulated mean concentration for Fe^{3+} and Mn^{2+} in $PM_{2.5}$ at the Beijing TSU site is 3.2 and 3.6 ng/m^3, respectively, and are smaller than the observed concentrations for soluble Fe and Mn (1.5-16 and 10-41 ng/m^3, respectively) in $PM_{2.5}$ at a Xi'an site (Wang et al., 2016). Note that Fe^{3+}/Mn^{2+} ions also have an anthropogenic source, and were estimated to account for 10-30% in Beijing (Shao et al., 2019). Furthermore, the soluble Fe/Mn speciation (including Fe^{3+}-Fe^{2+}, Mn^{2+}-Mn^{3+}-Mn^{4+} cycling) depends on dust mineralogy, particle acidity and heterogeneous redox reactions (Takahashi et al., 2011;Schroth et al., 2009), and is very difficult to be explicitly treated. Also the activity coefficients for Fe^{3+}/Mn^{2+} ions under the high ionic strength environment might differ (Cheng et al., 2016). The treatment of TMI pathway should be further improved in future studies."

References

Baker, A. R., Jickells, T. D., Witt, M., and Linge, K. L.: Trends in the solubility of iron, aluminium,

manganese and phosphorus in aerosol collected over the Atlantic Ocean, Marine Chemistry, 98, 43-58, 10.1016/j.marchem.2005.06.004, 2006.
Chen, D., Liu, Z., Fast, J., and Ban, J.: Simulations of sulfate–nitrate–ammonium (SNA) aerosols during the extreme haze events over northern China in October 2014, Atmos. Chem. Phys., 16, 10707-10724, 2016.
Chen, F., Zhang, X., Zhu, X., Zhang, H., Gao, J., and Hopke, P. K.: Chemical Characteristics of PM 2.5 during a 2016 Winter Haze Episode in Shijiazhuang, China, Aerosol and Air Quality Research, 17, 368-380, 2017.
Claquin, T., Schulz, M., and Balkanski, Y. J.: Modeling the mineralogy of atmospheric dust sources, J Geophys Res-Atmos, 104, 22243-22256, Doi 10.1029/1999jd900416, 1999.
Duvall, R. M., Majestic, B. J., Shafer, M. M., Chuang, P. Y., Simoneit, B. R. T., and Schauer, J. J.: The water-soluble fraction of carbon, sulfur, and crustal elements in Asian aerosols and Asian soils, Atmos. Environ., 42, 5872-5884, 10.1016/j.atmosenv.2008.03.028, 2008.
Herrmann, H., Ervens, B., Nowacki, P., Wolke, R., and Zellner, R.: A chemical aqueous phase radical mechanism for tropospheric chemistry, Chemosphere, 38, 1223-1232, 1999.
Herrmann, H., Tilgner, A., Barzaghi, P., Majdik, Z., Gligorovski, S., Poulain, L., and Monod, A.: Towards a more detailed description of tropospheric aqueous phase organic chemistry: CAPRAM 3.0, Atmospheric Environment, 39, 4351-4363, 2005.
Hsu, S. C., Wong, G. T. F., Gong, G. C., Shiah, F. K., Huang, Y. T., Kao, S. J., Tsai, F. J., Lung, S. C. C., Lin, F. J., Lin, I. I., Hung, C. C., and Tseng, C. M.: Sources, solubility, and dry deposition of aerosol trace elements over the East China Sea, Marine Chemistry, 120, 116-127, 10.1016/j.marchem.2008.10.003, 2010.
Johnson, M. S., Meskhidze, N., Solmon, F., Gasso, S., Chuang, P. Y., Gaiero, D. M., Yantosca, R. M., Wu, S. L., Wang, Y. X., and Carouge, C.: Modeling dust and soluble iron deposition to the South Atlantic Ocean, J Geophys Res-Atmos, 115, Artn D15202
10.1029/2009jd013311, 2010.
Journet, E., Desboeufs, K. V., Caquineau, S., and Colin, J. L.: Mineralogy as a critical factor of dust iron solubility, Geophysical Research Letters, 35, Artn L07805
10.1029/2007gl031589, 2008.
Meskhidze, N., Chameides, W., Nenes, A., and Chen, G.: Iron mobilization in mineral dust: Can anthropogenic SO2 emissions affect ocean productivity?, Geophysical Research Letters, 30, 2003.
Ravelo-Perez, L. M., Rodriguez, S., Galindo, L., Garcia, M. I., Alastuey, A., and Lopez-Solano, J.: Soluble iron dust export in the high altitude Saharan Air Layer, Atmos. Environ., 133, 49-59, 10.1016/j.atmosenv.2016.03.030, 2016.
Schroth, A. W., Crusius, J., Sholkovitz, E. R., and Bostick, B. C.: Iron solubility driven by speciation in dust sources to the ocean, Nature Geoscience, 2, 337-340, 10.1038/Ngeo501, 2009.
Shi, Z. B., Krom, M. D., Jickells, T. D., Bonneville, S., Carslaw, K. S., Mihalopoulos, N., Baker, A. R., and Benning, L. G.: Impacts on iron solubility in the mineral dust by processes in the source region and the atmosphere: A review, Aeolian Research, 5, 21-42, 10.1016/j.aeolia.2012.03.001, 2012.
Sun, Y., Zhuang, G., Tang, A. A., Wang, Y., and An, Z.: Chemical characteristics of PM2.5 and PM10 in haze-fog episodes in Beijing, Environ Sci Technol, 40, 3148-3155, 10.1021/es051533g, 2006.
Takahashi, Y., Higashi, M., Furukawa, T., and Mitsunobu, S.: Change of iron species and iron solubility in Asian dust during the long-range transport from western China to Japan, Atmos. Chem. Phys., 11, 11237-11252, 10.5194/acp-11-11237-2011, 2011.

Wang, G., Zhang, R., Gomez, M. E., Yang, L., Levy Zamora, M., Hu, M., Lin, Y., Peng, J., Guo, S., Meng, J., Li, J., Cheng, C., Hu, T., Ren, Y., Wang, Y., Gao, J., Cao, J., An, Z., Zhou, W., Li, G., Wang, J., Tian, P., Marrero-Ortiz, W., Secrest, J., Du, Z., Zheng, J., Shang, D., Zeng, L., Shao, M., Wang, W., Huang, Y., Wang, Y., Zhu, Y., Li, Y., Hu, J., Pan, B., Cai, L., Cheng, Y., Ji, Y., Zhang, F., Rosenfeld, D., Liss, P. S., Duce, R. A., Kolb, C. E., and Molina, M. J.: Persistent sulfate formation from London Fog to Chinese haze, Proc Natl Acad Sci U S A, 113, 13630-13635, 10.1073/pnas.1616540113, 2016.

Wang, Y., Zhuang, G. S., Sun, Y. L., and An, Z. S.: The variation of characteristics and formation mechanisms of aerosols in dust, haze, and clear days in Beijing, Atmos. Environ., 40, 6579-6591, 10.1016/j.atmosenv.2006.05.066, 2006.

Zheng, B., Zhang, Q., Zhang, Y., He, K. B., Wang, K., Zheng, G. J., Duan, F. K., Ma, Y. L., and Kimoto, T.: Heterogeneous chemistry: a mechanism missing in current models to explain secondary inorganic aerosol formation during the January 2013 haze episode in North China, Atmos. Chem. Phys., 15, 2031-2049, 10.5194/acp-15-2031-2015, 2015.

Response to Anonymous Referee #2

This study implemented a new aerosol water chemistry module (AWAC) in the WRF-Chem model, and aimed to understand the mechanisms of haze formation over China, in particular, to examine the relative roles of multiphase chemical reactions in aerosol water on particulate sulfate production, which is mainly related to the questions about aerosol pH. They investigated the spatial and temporal distributions of pH around Beijing with the model, and found that the rapid production of sulfate in the NCP can be maintained with the pH range of 4.2-5.7. This is a very interesting and important work. Scientifically, it is still under debate. The analysis of modeling results provided some evidence. However, I still have some questions about the uncertainty of results and the robustness of conclusion. More analysis and clarifications are needed before publication.

We thank the reviewer for the very valuable and constructive comments, which help us to improve the study and manuscript. Please find our point-by-point response (black) and the corresponding revisions (blue and *Italic*) below.

Specific Comments:

1. As the authors also agreed, the pH may be one of the key factors controlling the AWAC processes. However, unfortunately, there is no direct measurement of pH for evaluation. Currently, most studies used the model to calculate the pH, which makes the pH estimation dependent on modules. It is good to couple ISORROPIA II into WRF-Chem, but we still cannot rule out the dependence of pH calculation on this module. In WRF-Chem, the existing module for pH calculation is MOSAIC. Did the authors estimate the pH with MOSAIC and compare the values with ISORROPIA? Are they consistent?

Response:

Good question, thanks. In the original WRF-Chem model Version 3.8, both MADE/SORGAM/ISORROPIA aerosol scheme and MOSAIC aerosol scheme could be used to simulate the aerosol thermodynamics (including aerosol pH and water content). Previous field campaign studies have used the ISORROPIA II model to simulate the aerosol thermodynamics during the haze or non-haze periods in the North China Plain, and reported reasonable model performance (Song et al., 2018;Shi et al., 2017;Liu et al., 2017;Ding et al., 2019;Guo et al., 2017). However, the applicability of MOSAIC aerosol scheme specifically in simulating the aerosol thermodynamics in the North China Plain remains rarely reported. Thus in this study, we have chosen the MADE/SORGAM/ISORROPIA aerosol scheme, and further updated the default ISORROPIA model (Nenes et al., 1998) with the improved version (Fountoukis and Nenes, 2007;Song et al., 2018). The simulated mean pH for different scenarios in our study ranges between 4.2 and 5.7 in the North China Plain, and is comparable with the mean pH values reported in previous relevant studies (e.g., Liu et al., 2017;Shi et al., 2017;Song et al., 2018;Ding et al., 2019).

In the MOSAIC framework (Zaveri et al., 2008), the Multicomponent Equilibrium Solver for Aerosols (MESA) is used to simulate the aerosol thermodynamics (Zaveri et al., 2005a;Zaveri et al., 2005b). The algorithm of MESA model differs significantly from that of ISORROPIA II, including the chemical species involved (Potassium and Magnesium is excluded in MESA), determination of activity coefficient and mutual deliquescence relative humidity (MDRH), and the treatment of phase state and Kelvin Effect. Pye et al. (2020) has compared the pH values estimated by the box-model version of MOSAIC and ISORROPIA II (with the identical modeling input), and they found that the average aerosol pH differed

by 0.3 unit (the difference in pH could be up to 1 unit, and was greater with the decreasing relative humidity). It seems that there is no significant disparity in terms of predicting pH between models of MOSAIC and ISORROPIA. And we agree with the reviewer that it is very important and interesting to compare and analyze the results of different aerosol schemes during the severe haze episodes simulated in our study. But such issue is beyond the research scope of our current study, and it requires considerable efforts to couple the aerosol water chemistry module (AWAC) with the MOSAIC aerosol scheme. Nonetheless, we have added some relevant discussion as a caveat of our study in the Conclusion Section of the revised manuscript:

"Uncertainties relevant with the algorithms to solve the aerosol thermodynamics, including the treatment of non-ideality, size effects, phase state, mixing state, the interactions between inorganic compounds and organic compounds, as well as phase separation, should also be addressed in future studies."

2. For evaluation, since NH3 and NH4+ are so important in this AWAC system, could authors evaluate both of them? In Fig. 1, I didn't find the evaluation of NH4+ and NH3.

Response:

Good suggestion, thanks. Unfortunately, the observational data for ammonia concentrations in the North China Plain during January 2013 is unavailable. Nonetheless we have compared the simulated ammonia concentrations against the observations at other urban Beijing sites during the wintertime in other years:

Table R1. Modelled and observed NH_3, total NH_x (TNH_x) and fraction of NH_x in the particle phase (F_NH4) at urban Beijing sites [a].

	NH_3 mean (ppb)	NH_3 median (ppb)	TNH_x mean (ppb)	TNH_x median (ppb)	F_NH4 mean (%)	F_NH4 median (%)
MEIC_CTRL [b]	4.9	5.0	17.5	12.0	72	70
CTRL [b]	15.5	13.5	28.3	21.2	45	61
Meng et al. (2011) [c]	10.3	/	/	/	/	/
Liu et al. (2017) [d]	22.0	/	/	/	/	/
Song et al. (2018) [e]	/	18.0	/	39.1	/	54

[a] The modelling and measuring time differs, including months of November, December, January and February. Nonetheless, estimated emissions and observed concentrations of NH_3 in one study (e.g., Meng et al., 2011;Zhang et al., 2018) both have a minor difference among these months.
[b] Monthly mean value at Tsinghua University site (referred to Beijing site) during January of 2013.
[c] Mean value at Chinese Academy of Meteorological Sciences site during wintertime from 2008 to 2009.
[d] Mean value at Peking University site during November and December in both 2015 and 2016.
[e] Median value at Institute of Atmospheric Physics site from November to December of 2014.

As shown in Table R1, doubling the NH_3 emissions better match the observed ammonia and ammonium concentrations. Furthermore, Kong et al. (2019) estimated that the MEIC inventory (used as the anthropogenic emission inventory in our study) under-predicted NH_3 emissions by about 40% in the North China Plain. Thus, doubling the NH_3 emissions seems a reasonable assumption. We keep Table R1 in the Supplement, and further clarify this issue in the Section 2.2 of the revised manuscript:

"As shown in Table S7 of Supplement, compared with the scenario using the default MEIC emission data, the CTRL scenario (with doubled NH_3 emissions) better matches both the observed ammonia and ammonium concentrations at urban Beijing sites during wintertime (Meng et al., 2011;Liu et al., 2017;Song et al., 2018)."

In Fig. 2, for PM25_OCAT, why not evaluate the absolute values of each components such as K, MG, CA? The emission factor of OCAT is multiplied by 4.5 to match observation. How is this applied? Do you apply it to the total dust emission? This is a huge factor. Did you evaluate the dust mass/AOD over the dust source region to confirm this?

Response:

We thank the reviewer for raising this concern and the very good comment. The dust scheme we used is the improved GOCART dust scheme which is coupled with the MADE/SORGAM aerosol scheme. This dust scheme has been described and evaluated in Zhao et al. (2010) and Zhao et al. (2013). We do not change any of this dust scheme (i.e., the simulated total dust flux is unchanged). WRF/Chem prescribes a specific mass ratio of the fine mode dust emission to the total dust emission, and we further adopt the speciation fractions for the fine mode crustal particles of K, Na, Ca and Mg within the East Asian fine mode dust from Dong et al. (2016). However, Dong et al. (2016) indicated that observed fine particles have a considerably higher mass contribution within the East Asian dust than the chemical transport model (CTM) prescribes. With sensitivity tests, we found that multiply the fine mode dust speciation fractions for K, Na, Ca and Mg by merely one factor of 4.5 could better match the observed PM25_OCAT concentrations at Beijing TSU site.

We have clarified how to tune the PM25_OCAT concentrations in the second and third paragraph of Section 2.2 in the revised manuscript:

"WRF/Chem prescribes a specific mass ratio of the fine mode dust emission to the total dust emission, and we further adopt the fine mode dust emission speciation profiles from Dong et al. (2016). The mass fraction for fine particle components of K, Na, Ca, Mg, Fe and Mn minerals (denoted as PM25_K, PM25_NA, PM25_CA, PM25_MG, PM25_FE and PM25_MN, respectively) from dust source are set as 3.77%, 3.94%, 7.94%, 0.80%, 2.43%, and 0.063%, respectively."

"To match the observations of PM25_OCAT, the emissf_{OCAT} is set to 4.5 (the total dust emission is unchanged), and Dong et al. (2016) indicated that observed fine particles should have a considerably higher mass contribution within the East Asian dust than the chemical transport model prescribes."

Nonetheless, we have compared the simulated AOD_{550nm} with the MODIS as well as AERONET AOD_{550nm} data during January 2013. As shown in Figure R1, the MODIS AOD data is always missing in the vicinity of dust source regions (especially the Gobi Desert), while WRF/Chem simulated an AOD of ~0.2-0.4 there. The model could well reproduce the observed pattern in day-to-day changes of AOD downwind to the Western Pacific. But during the severely polluted episodes, the simulated AOD is not overestimated but rather underestimated especially over the Beijing-Tianjin-Hebei area. Moreover, the simulated AOD at the Dalanzadgad (the capital of SouthGobi Aimag in Mongolia) site is 0.027±0.007, and is also lower than the AERONET AOD data (https://aeronet.gsfc.nasa.gov/cgi-bin/draw_map_display_aod_v3) of 0.076. Results show that multiplying the fine mode dust speciation fractions for K, Na, Ca and Mg by a factor of 4.5 does not lead to the systematic overestimation of AOD. Even though large uncertainties exist for the simulation of dust events, the results of sensitivity tests in our study show that both the diurnal cycle pattern and vertical profile pattern for pH are consistent with varying dust emissions, meanwhile the rapid production of sulfate could be maintained.

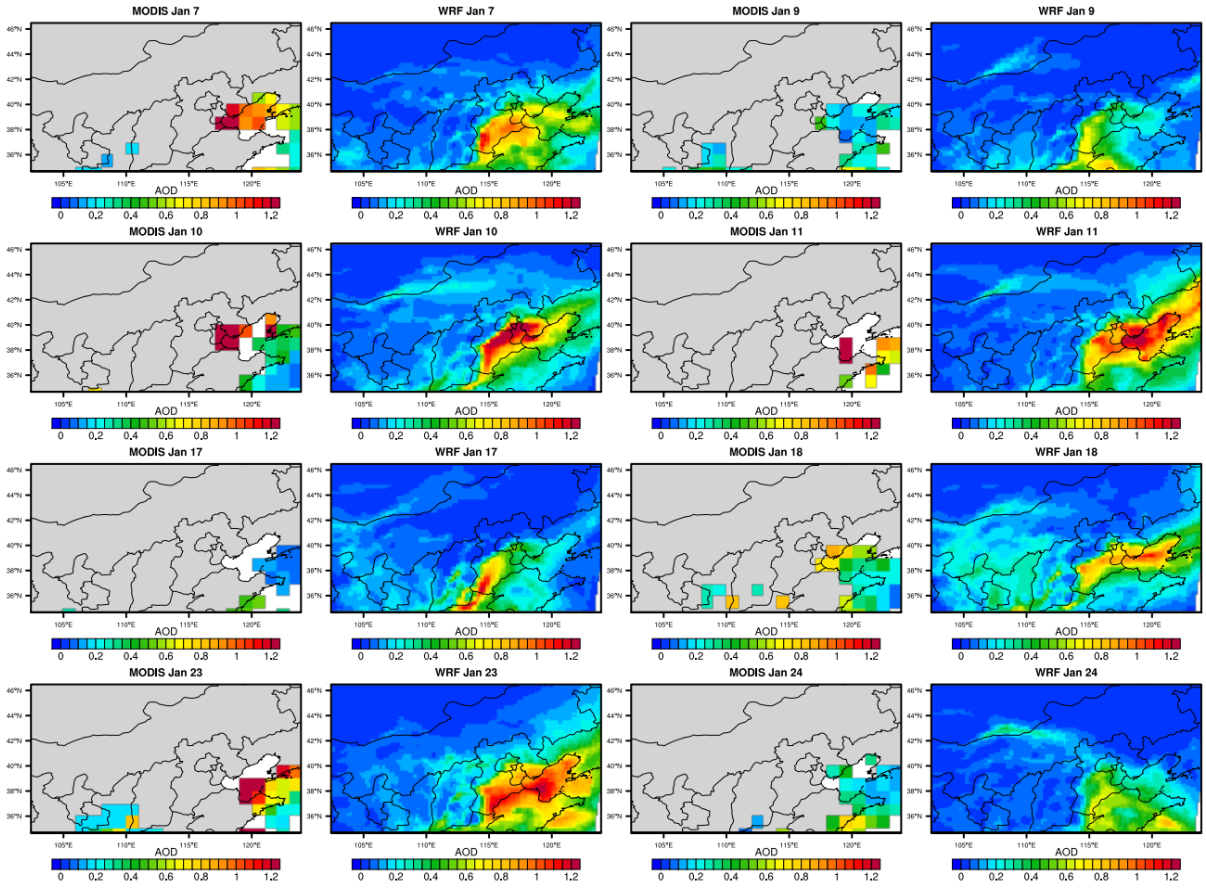

Figure R1. Comparison of MODIS AOD and simulated AOD during January of 2013.

Figure R2 compares the observed PM25_K, PM25_NA, PM25_MG, and PM25_CA with the simulated results (OBS vs. CTRL). The model in general reasonably predicts these individual crustal species, but with a slight overestimation of PM25_CA. We have conducted an additional control simulation tuned to match the observed PM25_K, PM25_MG, PM25_NA and PM25_CA at Beijing TSU site (OCAT_CTRL in Figure R2). The average pH at the surface in OCAT_CTRL case (5.0±0.6) is only about 0.2 unit lower than the CTRL case (5.2±0.5).

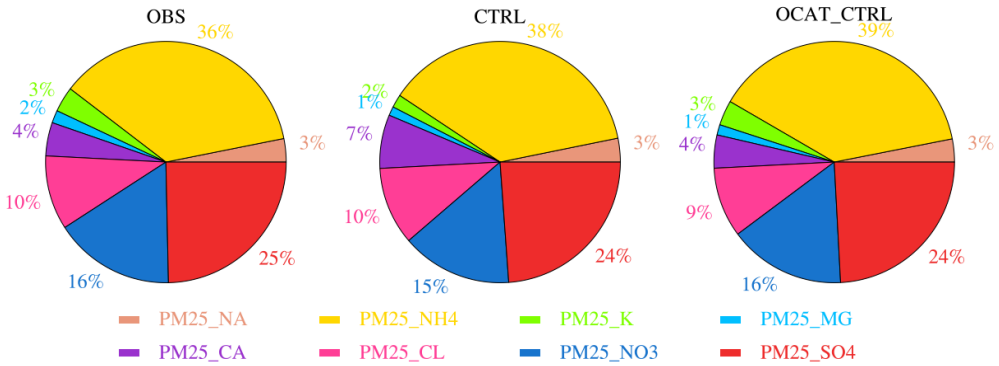

Figure R2. Observed (OBS) and simulated (scenarios of CTRL and OCAT_CTRL) mean electric charge fractions for fine particulate sulfate (PM25_SO4, using SO_4^{2-} as the surrogate), nitrate (PM25_NO3), ammonium (PM25_NH4), chloride (PM25_CL), sodium (PM25_NA), potassium (PM25_K), calcium (PM25_CA) and magnesium (PM25_MG) at TSU site during January of 2013.

3. In Fig. 1 and 2, although the added AWAC significantly increased sulfate production and the mean is closer to the observation, however, it is evident that the model still missed many events. This reflects that there are still some other important processes/mechanisms are missed in the model. Therefore, is it reasonable to use the observation to constrain the model AWAC process? i.e., there may be other processes contributing to the sulfate mass concentration more than AWAC? Please add some explanation and discussion.

Response:

Very good question, thanks. The importance of aerosol water phase production of sulfate has been widely accepted (Li et al., 2017;Chen et al., 2016;Zheng et al., 2015;Cheng et al., 2016;Zhang et al., 2015;Wang et al., 2016;Shao et al., 2019;Xue et al., 2019;Gen et al., 2019;Chen et al., 2019;Wu et al., 2019), and we think that during the severe haze episodes, implementing the heterogeneous reactions in aerosol water might be a key to reduce the gap between modelled sulfate concentrations and observations. After implementing the AWAC, the model performance is significantly improved, and the NMB between observed sulfate-nitrate-ammonium is reduced from -40%~-90% to ±5%. However, as pointed by the reviewer, discrepancies still remain in some events, which may be due to the uncertainties in the treatment of emission, transport (i.e., advection and turbulent mixing), removal (dry and wet deposition), and also the other potential sulfate formation pathways.

Our study focuses on investigating the characterises in the spatio-temporal distribution for aerosol pH as well as sulfate formation budget, and also the uncertainties relevant with assumptions for input parameters. In the CTRL scenario, we tune the input parameters relevant with concentrations for sulfate and other fine particle components (nitrate, ammonium, chlorides and crustal species) to better constrain the spatio-temporal distribution of aerosol pH. The different sources of uncertainties have been tested (Section 3.6). Specifically, we have used the observed sulfate to constrain the TMI formation pathway. Here, we have added one extra simulation of TMI0.5 (both FS_{FE3+} and FS_{MN2+} are halved) to further investigate the uncertainty relevant with TMI concentrations. As shown in Figure 9 of the revised manuscript, our conclusion in the manuscript regarding the diurnal cycle pattern and vertical profile pattern for aerosol pH, as well as the co-existence of multiple sulfate regime and how they interact with pH is consistent in the scenarios of TMI0, TMI0.5 and TMI2.

We have further clarified this issue in the third paragraph of Section 2.2 in the revised manuscript:

"The CTRL scenario is expected to reproduce the observed fine particle compositions (including sulfate, nitrate, ammonium, chloride and crustal components) and gas phase pollutants, and thus more reliably predict the spatio-temporal distribution of pH, AWC and sulfate production … Note that the assumption behind tuning only FS_{FE3+} and FS_{MN2+} to better agree with observed sulfates, is that the model could reasonably simulate the concentrations for other oxidants (e.g., OH, H_2O_2, O_3 and NO_2), thus the deviation from observation can be attributed to the uncertainties in representation of TMI pathway. Note that uncertainties in the emission, transport (i.e., advection and turbulent mixing), removal (dry and wet deposition) and sulfate formation in other phases could also contribute to the discrepancies between modeling results and observations. Nonetheless, this study does not aim at estimating the exact values for aerosol pH and sulfate formation budget. Instead, this study focuses on the characterises in the spatio-temporal distribution for aerosol pH as well as sulfate formation budget, and also the uncertainties relevant with assumptions for input parameters."

Related question, any evidence of significant contribution of AWAC on sulfate production in other events in recent year (2017, 2018, 2019)?

Response:

A very good and interesting question, thanks. The importance of aerosol water phase production of sulfate has been widely discussed and accepted (e.g., Li et al., 2017;Chen et al., 2016;Zheng et al., 2015;Cheng et al., 2016;Wang et al., 2016;Shao et al., 2019;Wu et al., 2019) during the severe haze episodes from early to middle 2010s (Table R2).

Table R2. Selection of the studies focusing on the heterogeneous reactions during the severe haze episodes from early to middle 2010s in China.

Reference	Study time period and area
Zheng et al. (2015)	January 2013 in Beijing–Tianjin–Hebei area
Chen et al. (2016)	October 2014 in North China Plain
Cheng et al. (2016)	January 2013 in Beijing
Wang et al. (2016)	17 November to 12 December of 2012 in Xi'an 21 January to 4 February of 2015 in Beijing
Li et al. (2017)	16 to 27 December 2013 in the Guanzhong basin 13 to 21 January 2014 in Beijing–Tianjin–Hebei area
Shao et al. (2019)	18 October 2014 to 17 January 2015 in the whole China
Wu et al. (2019)	Wintertime of 2015 in the North China Plain

However, the contribution of heterogeneous reactions to sulfate formation in recent years (2017-2020) remains rarely studied and quantified. Note that the air pollution over China has been remarkably mitigated in recent years since the implementation of Clean Air Action in 2013 (Fan et al., 2020;Zhang et al., 2019;Wang et al., 2019;Hou et al., 2019;Cheng et al., 2019). And Zheng et al. (2018) estimated that during 2013–2017, China's anthropogenic emissions decreased by ~60%, ~20% and ~35% for sulfur dioxide (SO_2), nitrogen oxides (NO_x) and $PM_{2.5}$, respectively. Unlike the negative feedback between aerosol loadings and their photochemical production (Kong et al., 2015), the multiphase reactions induce a positive feedback mechanism, i.e., higher particle matter levels lead to more aerosol water, which accelerates sulfate production and further increases the aerosol concentration (Cheng et al., 2016). The role of heterogeneous reactions might exhibit a weakening trend for the inter-annual variation with the decreasing emissions.

4. Line 21 of page 3, "except for" to "besides"?

Response:

Thanks for pointing out this typo, and we have corrected it.

5. Table 2, the description of scenarios includes "halved". It seems to me that there are only two cases: zero and doubled.

Response:

Thanks for pointing out this typo, and we have corrected it.

References:

Chen, D., Liu, Z., Fast, J., and Ban, J.: Simulations of sulfate–nitrate–ammonium (SNA) aerosols during the extreme haze events over northern China in October 2014, Atmos. Chem. Phys., 16, 10707-10724, 2016.

Chen, T., Chu, B., Ge, Y., Zhang, S., Ma, Q., He, H., and Li, S. M.: Enhancement of aqueous sulfate formation by the coexistence of NO2/NH3 under high ionic strengths in aerosol water, Environ Pollut, 252, 236-244, 10.1016/j.envpol.2019.05.119, 2019.

Cheng, J., Su, J., Cui, T., Li, X., Dong, X., Sun, F., Yang, Y., Tong, D., Zheng, Y., and Li, Y.: Dominant role of emission reduction in PM 2.5 air quality improvement in Beijing during 2013–2017: A model-based decomposition analysis, Atmos. Chem. Phys., 19, 6125-6146, 2019.

Cheng, Y., Zheng, G., Wei, C., Mu, Q., Zheng, B., Wang, Z., Gao, M., Zhang, Q., He, K., Carmichael, G., Poschl, U., and Su, H.: Reactive nitrogen chemistry in aerosol water as a source of sulfate during haze events in China, Sci Adv, 2, e1601530, 10.1126/sciadv.1601530, 2016.

Ding, J., Zhao, P. S., Su, J., Dong, Q., Du, X., and Zhang, Y. F.: Aerosol pH and its driving factors in Beijing, Atmos. Chem. Phys., 19, 7939-7954, 10.5194/acp-19-7939-2019, 2019.

Dong, X. Y., Fu, J. S., Huang, K., Tong, D., and Zhuang, G. S.: Model development of dust emission and heterogeneous chemistry within the Community Multiscale Air Quality modeling system and its application over East Asia, Atmos. Chem. Phys., 16, 8157-8180, 10.5194/acp-16-8157-2016, 2016.

Fan, H., Zhao, C., and Yang, Y.: A comprehensive analysis of the spatio-temporal variation of urban air pollution in China during 2014–2018, Atmos. Environ., 220, 117066, 2020.

Fountoukis, C., and Nenes, A.: ISORROPIA II: a computationally efficient thermodynamic equilibrium model for K^+–Ca^{2+}–Mg^{2+}–NH_4^+–Na^+–SO_4^{2-}–NO_3^-–Cl^-–H_2O aerosols, Atmospheric Chemistry and Physics, 7, 4639-4659, 2007.

Gen, M. S., Zhang, R. F., Huang, D. D., Li, Y. J., and Chan, C. K.: Heterogeneous Oxidation of SO2 in Sulfate Production during Nitrate Photolysis at 300 nm: Effect of pH, Relative Humidity, Irradiation Intensity, and the Presence of Organic Compounds, Environ. Sci. Technol., 53, 8757-8766, 10.1021/acs.est.9b01623, 2019.

Guo, H., Weber, R. J., and Nenes, A.: High levels of ammonia do not raise fine particle pH sufficiently to yield nitrogen oxide-dominated sulfate production, Sci. Rep., 7, 12109, 2017.

Hou, X., Zhu, B., Kumar, K. R., and Lu, W.: Inter-annual variability in fine particulate matter pollution over China during 2013–2018: Role of meteorology, Atmos. Environ., 214, 116842, 2019.

Kong, L., Tang, X., Zhu, J., Wang, Z., Pan, Y., Wu, H., Wu, L., Wu, Q., He, Y., and Tian, S.: Improved inversion of monthly ammonia emissions in China in combination of the Chinese Ammonia Monitoring Network and ensemble Kalman filter, Environ. Sci. Technol., 2019.

Kong, X., Forkel, R., Sokhi, R. S., Suppan, P., Baklanov, A., Gauss, M., Brunner, D., Barò, R., Balzarini, A., Chemel, C., Curci, G., Jiménez-Guerrero, P., Hirtl, M., Honzak, L., Im, U., Pérez, J. L., Pirovano, G., San Jose, R., Schlünzen, K. H., Tsegas, G., Tuccella, P., Werhahn, J., Žabkar, R., and Galmarini, S.: Analysis of meteorology–chemistry interactions during air pollution episodes using online coupled models within AQMEII phase-2, Atmos. Environ., 115, 527-540, 10.1016/j.atmosenv.2014.09.020, 2015.

Li, G. H., Bei, N. F., Cao, J. J., Huang, R. J., Wu, J. R., Feng, T., Wang, Y. C., Liu, S. X., Zhang, Q., Tie, X. X., and Molina, L. T.: A possible pathway for rapid growth of sulfate during haze days in China, Atmos. Chem. Phys., 17, 3301-3316, 10.5194/acp-17-3301-2017, 2017.

Liu, M. X., Song, Y., Zhou, T., Xu, Z. Y., Yan, C. Q., Zheng, M., Wu, Z. J., Hu, M., Wu, Y. S., and Zhu, T.: Fine particle pH during severe haze episodes in northern China, Geophysical Research Letters, 44, 5213-5221, 10.1002/2017gl073210, 2017.

Meng, Z. Y., Lin, W. L., Jiang, X. M., Yan, P., Wang, Y., Zhang, Y. M., Jia, X. F., and Yu, X. L.: Characteristics of atmospheric ammonia over Beijing, China, Atmos. Chem. Phys., 11, 6139-6151, 10.5194/acp-11-6139-2011, 2011.

Nenes, A., Pandis, S. N., and Pilinis, C.: ISORROPIA: A new thermodynamic equilibrium model for multiphase multicomponent inorganic aerosols, Aquatic geochemistry, 4, 123-152, 1998.

Pye, H. O. T., Nenes, A., Alexander, B., Ault, A. P., Barth, M. C., Clegg, S. L., Collett, J. L., Fahey, K. M., Hennigan, C. J., Herrmann, H., Kanakidou, M., Kelly, J. T., Ku, I. T., McNeill, V. F., Riemer, N., Schaefer, T., Shi, G. L., Tilgner, A., Walker, J. T., Wang, T., Weber, R., Xing, J., Zaveri, R. A., and Zuend, A.: The acidity of atmospheric particles and clouds, Atmos. Chem. Phys., 20, 4809-4888, 10.5194/acp-20-4809-2020, 2020.

Shao, J. Y., Chen, Q. J., Wang, Y. X., Lu, X., He, P. Z., Sun, Y. L., Shah, V., Martin, R. V., Philip, S., Song, S. J., Zhao, Y., Xie, Z. Q., Zhang, L., and Alexander, B.: Heterogeneous sulfate aerosol formation mechanisms during wintertime Chinese haze events: air quality model assessment using observations of sulfate oxygen isotopes in Beijing, Atmos. Chem. Phys., 19, 6107-6123, 10.5194/acp-19-6107-2019, 2019.

Shi, G., Xu, J., Peng, X., Xiao, Z., Chen, K., Tian, Y., Guan, X., Feng, Y., Yu, H., Nenes, A., and Russell, A. G.: pH of Aerosols in a Polluted Atmosphere: Source Contributions to Highly Acidic Aerosol, Environ Sci Technol, 51, 4289-4296, 10.1021/acs.est.6b05736, 2017.

Song, S. J., Gao, M., Xu, W. Q., Shao, J. Y., Shi, G. L., Wang, S. X., Wang, Y. X., Sun, Y. L., and McElroy, M. B.: Fine-particle pH for Beijing winter haze as inferred from different thermodynamic equilibrium models, Atmos. Chem. Phys., 18, 7423-7438, 10.5194/acp-18-7423-2018, 2018.

Wang, G., Zhang, R., Gomez, M. E., Yang, L., Levy Zamora, M., Hu, M., Lin, Y., Peng, J., Guo, S., Meng, J., Li, J., Cheng, C., Hu, T., Ren, Y., Wang, Y., Gao, J., Cao, J., An, Z., Zhou, W., Li, G., Wang, J., Tian, P., Marrero-Ortiz, W., Secrest, J., Du, Z., Zheng, J., Shang, D., Zeng, L., Shao, M., Wang, W., Huang, Y., Wang, Y., Zhu, Y., Li, Y., Hu, J., Pan, B., Cai, L., Cheng, Y., Ji, Y., Zhang, F., Rosenfeld, D., Liss, P. S., Duce, R. A., Kolb, C. E., and Molina, M. J.: Persistent sulfate formation from London Fog to Chinese haze, Proc Natl Acad Sci U S A, 113, 13630-13635, 10.1073/pnas.1616540113, 2016.

Wang, Y., Li, W., Gao, W., Liu, Z., Tian, S., Shen, R., Ji, D., Wang, S., Wang, L., and Tang, G.: Trends in particulate matter and its chemical compositions in China from 2013–2017, Science China Earth Sciences, 62, 1857-1871, 2019.

Wu, J., Bei, N., Hu, B., Liu, S., Zhou, M., Wang, Q., Li, X., Liu, L., Feng, T., and Liu, Z.: Is water vapor a key player of the wintertime haze in North China Plain?, Atmos. Chem. Phys., 19, 8721-8739, 2019.

Xue, J., Yu, X., Yuan, Z. B., Griffith, S. M., Lau, A. K. H., Seinfeld, J. H., and Yu, J. Z.: Efficient control of atmospheric sulfate production based on three formation regimes, Nature Geoscience, 12, 977-+, 10.1038/s41561-019-0485-5, 2019.

Zaveri, R. A., Easter, R. C., and Peters, L. K.: A computationally efficient multicomponent equilibrium solver for aerosols (MESA), Journal of Geophysical Research: Atmospheres, 110, 2005a.

Zaveri, R. A., Easter, R. C., and Wexler, A. S.: A new method for multicomponent activity coefficients of electrolytes in aqueous atmospheric aerosols, Journal of Geophysical Research: Atmospheres, 110, 2005b.

Zaveri, R. A., Easter, R. C., Fast, J. D., and Peters, L. K.: Model for simulating aerosol interactions and chemistry (MOSAIC), Journal of Geophysical Research: Atmospheres, 113, 2008.

Zhang, L., Chen, Y. F., Zhao, Y. H., Henze, D. K., Zhu, L. Y., Song, Y., Paulot, F., Liu, X. J., Pan, Y. P., Lin, Y., and Huang, B. X.: Agricultural ammonia emissions in China: reconciling bottom-up and top-

down estimates, Atmos. Chem. Phys., 18, 339-355, 10.5194/acp-18-339-2018, 2018.
Zhang, Q., Zheng, Y., Tong, D., Shao, M., Wang, S., Zhang, Y., Xu, X., Wang, J., He, H., and Liu, W.: Drivers of improved PM2. 5 air quality in China from 2013 to 2017, P. Natl. Acad, Sci., 116, 24463-24469, 2019.
Zhang, R., Wang, G., Guo, S., Zamora, M. L., Ying, Q., Lin, Y., Wang, W., Hu, M., and Wang, Y.: Formation of urban fine particulate matter, Chem Rev, 115, 3803-3855, 10.1021/acs.chemrev.5b00067, 2015.
Zhao, C., Liu, X., Leung, L., Johnson, B., McFarlane, S. A., Gustafson Jr, W., Fast, J. D., and Easter, R.: The spatial distribution of mineral dust and its shortwave radiative forcing over North Africa: modeling sensitivities to dust emissions and aerosol size treatments, Atmos. Chem. Phys., 10, 8821, 2010.
Zhao, C., Chen, S., Leung, L., Qian, Y., Kok, J., Zaveri, R., and Huang, J.: Uncertainty in modeling dust mass balance and radiative forcing from size parameterization, Atmos. Chem. Phys., 13, 10733-10733, 2013.
Zheng, B., Tong, D., Li, M., Liu, F., Hong, C. P., Geng, G. N., Li, H. Y., Li, X., Peng, L. Q., Qi, J., Yan, L., Zhang, Y. X., Zhao, H. Y., Zheng, Y. X., He, K. B., and Zhang, Q.: Trends in China's anthropogenic emissions since 2010 as the consequence of clean air actions, Atmos. Chem. Phys., 18, 14095-14111, 10.5194/acp-18-14095-2018, 2018.
Zheng, G. J., Duan, F. K., Su, H., Ma, Y. L., Cheng, Y., Zheng, B., Zhang, Q., Huang, T., Kimoto, T., Chang, D., Poschl, U., Cheng, Y. F., and He, K. B.: Exploring the severe winter haze in Beijing: the impact of synoptic weather, regional transport and heterogeneous reactions, Atmos. Chem. Phys., 15, 2969-2983, 10.5194/acp-15-2969-2015, 2015.

Aerosol pH and chemical regimes of sulfate formation in aerosol water during winter haze in the North China Plain

Wei Tao[1,2], Hang Su[1*], Guangjie Zheng[2], Jiandong Wang[2], Chao Wei[1], Lixia Liu[2], Nan Ma[3], Meng Li[1], Qiang Zhang[4], Ulrich Pöschl[1], Yafang Cheng[2,1*]

[1]Multiphase Chemistry Department, Max Planck Institute for Chemistry, Mainz 55128, Germany
[2]Minerva Research Group, Max Planck Institute for Chemistry, Mainz 55128, Germany
[3]Institute for Environmental and Climate Research, Jinan University, Guangzhou 511443, China
[4]Department of Earth System Science, Tsinghua University, Beijing 100084, China

Correspondence to: H. Su (h.su@mpic.de) or Y. Cheng (yafang.cheng@mpic.de)

Abstract

Understanding the mechanism of haze formation is crucial for the development of deliberate pollution control strategies. Multiphase chemical reactions in aerosol water have been suggested as an important source of particulate sulfate during severe haze (Cheng et al., 2016;Wang et al., 2016). While the key role of aerosol water has been commonly accepted, the relative importance of different oxidation pathways in the aqueous phase is still under debate, mainly due to questions about aerosol pH. To investigate the spatio-temporal variability of aerosol pH and sulfate formation during winter in the North China Plain (NCP), we have developed a new aerosol water chemistry module (AWAC) for the WRF-Chem model (Weather Research and Forecasting model coupled with Chemistry). Using the WRF-Chem-AWAC model, we performed a comprehensive survey of the atmospheric conditions characteristic for wintertime in the NCP, focusing on January 2013. We find that aerosol pH exhibited a strong vertical gradient and distinct diurnal cycle, which was closely associated with the spatio-temporal variation in the relative abundance of acidic and alkaline fine particle components and their gaseous counterparts. Over Beijing, the average aerosol pH at the surface layer was ~5.4 and remained nearly constant around ~5 up to ~2 km above ground level; further aloft, the acidity rapidly increased to pH ~0 at ~3 km. The pattern of aerosol acidity increase with altitude persisted over the NCP, while the specific levels and gradients of pH varied between different regions. In the region north of ~41°N, the mean pH values at surface level were typically >6 and the main pathway of sulfate formation in aerosol water was S(IV) oxidation by ozone. South of ~41°N, the mean pH values at surface level were typically in the range of 4.4 to 5.7, and different chemical regimes and reaction pathways of sulfate formation prevailed in four different regions, depending on reactant concentrations and atmospheric conditions. The NO_2 reaction pathway

prevailed in the megacity region of Beijing and the large area of Hebei Province to the south and west of Beijing, as well as part of Shandong Province. The transition metal ion (TMI) pathway dominated in the inland region to the west and the coastal regions to the east of Beijing, and the H_2O_2 pathway dominated in the region extending further south (Shandong and Henan Provinces). In all of these regions, the O_3 and TMI pathways in aerosol water as well as the gas-particle partitioning of H_2SO_4 vapor became more important with increasing altitude. Although pH is sensitive to the abundance of NH_3 and crustal particles, we show that the rapid production of sulfate in the NCP can be maintained over a wide range of aerosol acidity (e.g., pH = 4.2-5.7) with transitions from TMI pathway dominated to NO_2/O_3 pathway dominated regimes.

Keywords: Winter haze, aerosol pH, multiphase chemistry, sulfate formation regime

1. Introduction

Persistent haze shrouding Beijing and its surrounding areas in North China Plain during cold winter is one of the most urgent and challenging environmental problems in China (Sun et al., 2014;Zheng et al., 2015b;Cheng et al., 2016). The winter haze often has the following characteristic features, including stagnant meteorological conditions, high relative humidity and high concentrations of $PM_{2.5}$ as well as elevated contributions of secondary inorganics in $PM_{2.5}$ (Zhang et al., 2014;Brimblecombe, 2012;Zheng et al., 2015b;Sun et al., 2014). Though extremely sharp increases in $PM_{2.5}$ concentration in Beijing (e.g., several hundred $\mu g\ m^{-3}\ h^{-1}$) have been attributed mainly to the transport processes rather than local chemical production, the large gap between modeled and observed $PM_{2.5}$ reveals that there are still missing chemical formation pathways in the state-of-the-art atmospheric chemical transport models (Zheng et al., 2015b;Cheng et al., 2016). Cheng et al. (2016) suggested and quantified that during severe haze multiphase reactions in aerosol water can produce remarkable amount of sulfate over a wide range of aerosol pH, which complements or even exceeds the contribution from gas phase and cloud chemistry during the haze events. Laboratory studies of Wang et al. (2016) provide an experimental proof for importance of NO_2 oxidation pathway in sulfate formation in aerosol water. However, depending on the aerosol pH and pollutant compositions, the major multiphase oxidation pathways may change from reactions of NO_2 and O_3 at pH > 4.5 to O_2 (catalyzed by Transition Metal Ion, TMI) and H_2O_2 at pH<4.5 (Cheng et al., 2016). Unlike the negative feedback between aerosol loadings and their photochemical production (Makar et al., 2015;Kong et al., 2015), the multiphase reactions induce a positive feedback mechanism, i.e., higher particle matter levels lead to more aerosol water, which accelerates sulfate production and further increases the aerosol concentration (Cheng et al., 2016).

Though the importance of reactions in aerosol water during severe haze has been widely accepted (Li et al., 2017a;Chen et al., 2016;Zheng et al., 2015b;Cheng et al., 2016;Zhang et al., 2015;Wang et al., 2016;Shao et al., 2019;Xue et al., 2019;Gen et al., 2019;Chen et al., 2019;Wu et al., 2019), the exact formation pathway is still under debate. Besides the aforementioned reactions (i.e., reactions of NO_2, O_3, TMI and H_2O_2), heterogeneous production of hydroxymethanesulfonate (HMS) by SO_2 and HCHO has also been proposed to contribute to the unexplained sulfate by models (Song et al., 2019;Moch et al., 2018). To a certain extent, this is not a surprise considering the strong dependence of multiphase reaction rate on aerosol pH and pollutant compositions (including the most important oxidants for sulfate formation). Hourly-predicted pH based on observations and thermodynamic model calculations showed a large variability from 2 to 8 in northern China (Shi et al., 2017;Ding et al., 2019). Previous observational and modeling studies also indicated that the temporal and spatial distribution of oxidants/catalysts, e.g., O_3 (Dufour et al., 2010;Xu et al., 2008), NO_2 (Zhang et al., 2012;Zhang et al., 2007) and TMI (Dong et al., 2016), were highly variable.

Thus, we hypothesize that multiple oxidation regimes for sulfate formation may indeed co-exist in the North China Plain. The apparent contrasting results could be a consequence of regime transitions between different locations and periods. To test our hypothesis, we have developed a new aerosol water chemistry module (AWAC) and implemented an improved version of ISORROPIA II into the WRF-Chem model (Weather Research and Forecasting model coupled with Chemistry) to better account for the different sulfate formation pathways. With a comprehensive model survey, we focus on the variabilities of aerosol pH and regimes of sulfate formation in aerosol water, aiming at reconciling the continuing debates on the dominate sulfate formation pathways in North China Plain. Detailed method description and model evaluation are provided in Section 2, followed by the results and discussion in Section 3. The last section summarizes the main conclusions and implications of this study.

2. Method

2.1 WRF-Chem-AWAC: new aerosol water chemistry module for WRF-Chem

To account for the formation of sulfate and nitrate in the liquid water of fine particles (including Aitken and accumulation modes, and denoted as $PM_{2.5}$), we have developed a new aerosol water chemistry module (AWAC) into WRF-Chem (version 3.8) (Grell et al., 2005). The coarse mode aerosols have been greatly simplified in MADE/SORGAM framework and the AWAC module is therefore not implemented for coarse mode aerosols. For sulfate (denoted as PM25_SO4) formation, we use explicit mechanisms involving 11 irreversible reactions for the oxidation of S(IV) by dissolved O_3, H_2O_2, TMI (only Fe^{3+} and Mn^{2+} are considered), NO_2 and CH_3OOH, respectively (Table 1). Mass transfer of SO_2 and gaseous oxidants between gas and liquid phase, as well as dissociation equilibrium of sulfurous acid are treated as irreversible reactions, and solved simultaneously with the redox reactions using KPP software (Damian et al., 2002;Sandu and Sander, 2006) and Rosenbrock solver (Sandu et al., 1997;Shampine, 1982). The formula for mass transfer rate coefficient, k_T (in unit of $cm \cdot s^{-1}$) is adopted from Jacob and Brasseur (2017):

$$k_T = \left(\frac{R_d}{D_g} + \frac{0.04}{\alpha\sqrt{8RT/\pi M_w}}\right)^{-1} \quad (1)$$

where R_d is the mean radius for fine particles (including aerosol water, with a unit of cm), D_g is the molecular diffusion coefficient ($cm^2 \cdot s^{-1}$), R is the gas constant (8.314 $J \cdot mol^{-1} \cdot K^{-1}$), T is the air temperature (K), M_w is the molecular weight ($kg \cdot mol^{-1}$), and α is the mass accommodation coefficient (unitless). Detailed descriptions are provided in the Supplement (Fig. S1-S5 and Tables S1-S5). Though using different solvers, the box model version of the aerosol water chemistry module could well reproduce the results in Cheng et al. (2016) (shown in Fig. S5 of Supplement).

Following Zheng et al. (2015a) and Chen et al. (2016), a parameterization scheme is adopted to simulate the aqueous phase production of nitrate (denoted as PM25_NO3):

$$\frac{dC_{\mathrm{PM25\_NO3}}}{dt} = \left(\frac{R_d}{D_{g,\mathrm{NO_2}}} + \frac{0.04}{\gamma_{\mathrm{NO_2}}\sqrt{8RT/\pi M_{w,\mathrm{NO_2}}}}\right)^{-1} \cdot Aa \cdot C_{\mathrm{NO_2(g)}} \quad (2)$$

where *Aa* is the surface area concentration for fine particles ($cm^2 \cdot cm^{-3}$), and γ is the uptake coefficient (unitless) for NO_2. γ has a lower limit (3.0×10^{-6}) and a higher limit (13.0×10^{-6}) when the RH is lower than 50 % and higher than 90 %, respectively. Note that the γ has been scaled 15 times lower than that used in Zheng et al. (2015a) to better match the observed PM25_NO3 with R = 0.74 and NMB = 3% (see more details in Sect. 3.1). When the RH ranges between 50 % and 90 %, the value for γ is then linearly interpolated between the two limits.

To simulate aerosol water content (AWC) and pH, as input parameters of the AWAC module, we have replaced the original ISORROPIA model in WRF-Chem with an improved version of ISORROPIA II (Fountoukis and Nenes, 2007;Song et al., 2018). The source code of the improved ISORROPIA II is available at http://wiki.seas.harvard.edu/geos-chem/index.php/ISORROPIA_II. ISORROPIA predicts the thermodynamic equilibrium (including pH) for an internal-mixed system of multiple inorganic components at a specific temperature and humidity. Following Ding et al. (2019), we assume that the phase state for aerosol is metastable at RH > 30%, otherwise the phase state is stable. If the predicted AWC is less than an infinitesimal value (the threshold value of 10^{-8} μg/m^3 is used, see Fig. S6 and S7 of Supplement for relevant uncertainties), pH is set to a missing value, and heterogeneous reactions in aerosol water are not calculated. Otherwise the heterogeneous oxidation module is called, assuming a fixed number/size distribution and thermodynamic status (including AWC and pH) within one time step of master chemistry module in WRF-Chem program.

RACM mechanism (Stockwell et al., 1997;Stockwell et al., 1990) is used to calculate the gas phase photochemistry, and provides the concentrations of gaseous precursors (e.g., SO_2, NO_2 etc.) and oxidants (e.g., O_3, H_2O_2 etc.). MADE/SORGAM scheme (Ackermann et al., 1998;Schell et al., 2001) with the improved ISORROPIA II model is used to simulate the aerosol dynamics (including nucleation, coagulation and condensation) and thermodynamics, and provide the aerosol size distribution, number concentration, as well as AWC and pH values. The Integrated process rate (IPR) technique (Tao et al., 2017;Tao et al., 2015) is used to record the formation rates of sulfuric and nitric acid vapor through photochemical oxidation in the gas phase.

For the TMI oxidation pathway, we assume that Fe^{3+} and Mn^{2+} will not be consumed in the TMI pathway due to the catalytic nature of Fe^{3+}/Mn^{2+}. The concentrations of Fe^{3+} and Mn^{2+} (in unit of mol/L) in aerosol water can be calculated by Eq. (3),

$$\begin{cases}[Fe^{3+}] = Min(C_{PM25\_FE} \cdot FS_{FE3+} / AWC, 2.6\times10^{-38} / [OH^-]^3) \\ [Mn^{2+}] = Min(C_{PM25\_MN} \cdot FS_{MN2+} / AWC, 1.6\times10^{-13} / [OH^-]^2)\end{cases} \quad (3)$$

where PM25_FE and PM25_MN are the fine particle components of Fe and Mn minerals, respectively, *C* denotes the concentrations in unit of mol per liter of air, FS_{FE3+} and FS_{MN2+} represent the maximum fractional solubility of Fe^{3+} and Mn^{2+}, respectively (regardless of the acidity of aerosol water), and *AWC* is the aerosol liquid water content in unit of liter per liter of air.

2.2 WRF-Chem model configuration and scenarios

The modeling framework is constructed on a single domain of 100 (west-east) × 70 (south-north) × 30 (vertical layers) grid cells with a horizontal resolution of 20 km (including the Gobi deserts, see Fig. S8 of Supplement). The overview of the chemical and physical options used in this study is summarized in Table S6 of Supplement. Madronich F-TUV photolysis scheme (Madronich, 1987) is used to calculate the photolysis rates. The initial and boundary conditions for meteorology and chemistry are derived from 1.0°×1.0° NCEP FNL data and global-scale MOZART outputs, respectively. Observation nudging (Liu et al., 2005) is used to nudge the modeled temperature, wind fields and humidity towards the observations (including surface and upper layers). Multi-resolution Emission Inventory for China (MEIC) of the year 2013 (MEIC, Lei et al., 2011;Zhang et al., 2009;Li et al., 2014;Li et al., 2017b) is used for anthropogenic emissions. The Megan scheme (Guenther et al., 2006) is used for biogenic VOCs emissions. The hourly biomass burning emissions data are provided by the Fire Inventory from NCAR (FINN, Wiedinmyer et al., 2010). We use the GOCART dust scheme (Ginoux et al., 2001;Zhao et al., 2010;Zhao et al., 2013), which is coupled with the MADE/SORGAM aerosol scheme.

In this study, we have simulated 15 scenarios as detailed in Table 2, including an ORIG scenario with WRF-Chem (original chemistry) and default emissions as mentioned above, a CTRL scenario with WRF-Chem-AWAC (with implementation of aerosol water aqueous phase chemistry) and optimized ammonia emission, as well as additional emissions for chloride and crustal fine particles, and 13 sensitivity scenarios with respect to CTRL scenario. Since anthropogenic source chlorine is not included in MEIC, we adopt the chlorine inventory in Liu et al. (2018), which provides the emissions of HCl from coal consumption. WRF/Chem prescribes a specific mass ratio of the fine mode dust emission to the total dust emission, and we further adopt the fine mode dust emission speciation profiles from Dong et al. (2016). The mass fraction for fine particle components of K, Na, Ca, Mg, Fe and Mn minerals (denoted as PM25_K, PM25_NA, PM25_CA, PM25_MG, PM25_FE and PM25_MN, respectively) from dust source are set as 3.77%, 3.94%, 7.94%, 0.80%, 2.43%, and 0.063%, respectively. Dry and wet depositions are also considered for these newly-added crustal fine particle components as detailed in Sect. 1.3 of Supplement.

The CTRL scenario is expected to reproduce the observed fine particle compositions (including sulfate, nitrate, ammonium, chloride and crustal components) and gas phase pollutants, and thus more reliably predict the spatio-temporal distribution of pH, AWC and sulfate production. For this purpose, five parameters in the CTRL scenario have been adjusted to better match the observations (with the criteria that the relative error of the monthly mean concentrations for different fine particle components is less than 5%), namely the factor multiplied to the anthropogenic ammonia emissions (denoted as $emissf_{NH3}$), the factor multiplied to dust speciation fractions for PM25_K, PM25_NA, PM_CA and PM25_MG (denoted as $emissf_{OCAT}$), the factor multiplied to the anthropogenic chloride emissions (denoted as $emissf_{CL}$), as well as FS_{FE3+} and FS_{MN2+} (the maximum fractional solubility of Fe^{3+} and Mn^{2+} in Eq. 3, respectively). In the CTRL scenario, $emissf_{NH3}$ has been set to 2, as recent studies using top-down inverse modeling (Van Damme et al., 2018;Zhang et al., 2018a;Wang et al., 2018;Kong et al., 2019) and direct measurement (Wang et al., 2018) found that previous bottom-up inventories might underestimate the NH_3 emissions, and MEIC inventory was estimated to under-predict NH_3 emissions by about 40% over the North China Plain (Kong et al., 2019). As shown in Table S7 of Supplement, compared with the scenario using the default MEIC emission data, the CTRL scenario (with doubled NH_3 emissions) better matches both the observed ammonia and ammonium concentrations at urban Beijing sites during wintertime (Meng et al., 2011;Liu et al., 2017;Song et al., 2018). To match the observations of PM25_OCAT, the $emissf_{OCAT}$ is set to 4.5 (the total dust emission is unchanged), and Dong et al. (2016) indicated that observed fine particles should have a considerably higher mass contribution within the East Asian dust than the chemical transport model prescribes. And $emissf_{CL}$ is set to 6 to match the observations of PM25_CL. To have a better agreement with the sulfate observation, FS_{FE3+} and FS_{MN2+} are set to 7% and 40%, respectively. Note that the assumption behind tuning only FS_{FE3+} and FS_{MN2+} to better agree with observed sulfates, is that the model could reasonably simulate the concentrations for other oxidants (e.g., OH, H_2O_2, O_3 and NO_2), thus the deviation from observation can be attributed to the uncertainties in representation of TMI pathway. Note that uncertainties in the emission, transport (i.e., advection and turbulent mixing), removal (dry and wet deposition) and sulfate formation in other phases could also contribute to the discrepancies between modeling results and observations. Nonetheless, this study does not aim at estimating the exact values for aerosol pH and sulfate formation budget . Instead, this study focuses on investigating the characterises in the spatio-temporal distribution for aerosol pH as well as sulfate formation budget, and also the uncertainties relevant with assumptions for input parameters. Journet et al. (2008) found that the dust mineralogy was a critical factor for iron solubility, and fractional Fe solubility was observed to be ~4% and less than 1% for samples of clay and iron (hydr-)oxides, respectively. A low fractional Fe solubility approximately or below 0.05% was reported for the non-atmospherically-processed arid soil samples (Schroth et al., 2009;Johnson et al., 2010;Shi et al., 2012). Most of Fe minerals exist in the form of hematite (α-Fe_2O_3) over the Gobi deserts (Claquin et al., 1999), and fractional Fe solubility was increased to 1-2% after 3–5 days transport from the Gobi deserts

(Meskhidze et al., 2003). A higher fractional Fe solubility up to ~10% was reported after a longer time of atmospheric aging for dust particles (Takahashi et al., 2011;Shi et al., 2012). Fractional Mn solubility for dust particles was observed to range between 20% and 60% (Duvall et al., 2008;Baker et al., 2006;Hsu et al., 2010). The rest 13 scenarios are used for sensitivity analysis on the uncertainties in $emissf_{NH3}$, $emissf_{OCAT}$, $emissf_{CL}$, FS_{FE3+} and FS_{MN2+}, as well as phase state assumption.

3. Results and discussion

3.1 Comparison of CTRL and ORIG scenarios

Figure 1 shows the comparison of ORIG and CTRL scenarios against observations obtained at the site located on the campus of Tsinghua University in Beijing (denoted as Beijing TSU site, 40°00'17"N, 116°19'34"E, ~10m height) during January 2013. The hourly data include online observations of concentrations of SO_2, PM25_SO4, NO_x (=NO+NO_2), PM25_NO3, O_3 and $PM_{2.5}$, as well as relative humidity (RH) that is closely related to the AWC. Details about the measurements have been described in Zheng et al. (2015b) and Cheng et al. (2016). As shown in Fig. 1, simulations from both scenarios were capable of reproducing the concentration levels of the sum of SO_2 and PM25_SO4, the sum of NO_x and PM25_NO3, O_3 and $PM_{2.5}$ with the normalized mean bias (NMB) around ±30% and the correlation coefficients (R) ranging between 0.5 and 0.7. The simulated RH well matched the observations with a NMB of ~12% and a R of ~0.9. Simulations of PM25_SO4, PM25_NO3 have been significantly improved in CTRL scenario.

Offline observations of PM25_K, PM25_NA, PM25_CA, PM25_MG, PM25_CL, PM25_SO4, PM25_NO3 and PM25_NH4 are also available in a daily basis (Zheng et al., 2015b;Cheng et al., 2016). As shown in Fig. 2, simulations of sulfate, nitrate and ammonium in $PM_{2.5}$ were greatly improved in the CTRL scenario, with a NMB within ±5%, while the NMB of the ORIG scenario was -90% for sulfate, -35% for nitrate and -65% for ammonium, respectively. The only source of PM25_CL in ORIG scenario was sea salt emissions, and it was negligible. The improved model WRF-Chem-AWAC with additional chloride emissions from coal combustion could capture the observed PM25_CL with a NMB of only ~10%. Other inorganic cations in $PM_{2.5}$ (denoted as PM25_OCAT, and only involves PM25_K, PM25_NA, PM25_CA and PM25_MG) were not included in original MADE/SORGAM scheme, and thus their concentrations were zero in ORIG scenario. The CTRL scenario could moderately reproduce the concentrations of PM25_OCAT with a NMB of ~60%. Note that the emission of PM25_OCAT has been adjusted based on the criterial of reducing the mismatch of simulation and observation within 5% on a monthly mean basis, and here the NMB here was calculated based on daily values.

As shown in the lower panel of Fig. 2, among the fine particle components mentioned above, observed PM25_NH4 and PM25_OCAT accounted for about 75% and 25% of the monthly mean ionic charge budget for cations, respectively. Observed PM25_CL, PM25_NO3 and PM25_SO4 accounted for about 20%, 32% and 48% of the monthly mean ionic charge budget for anions, respectively. The CTRL scenario could well capture the observed ionic charge budget, except that the mole fraction of PM25_CA in PM25_OCAT was slightly overestimated (PM25_CA had a higher mass fraction for dust emission speciation). Thus, in the following sections, the CTRL configuration is used to study the temporal and spatial distribution of aerosol pH and the regime transition of sulfate formation in aerosol water during winter haze events in North China Plain.

3.2 Vertical profile of pH over Beijing

Figure 3a shows the vertical profile of the simulated aerosol pH over Beijing site. The mean pH at surface layer was ~5.4 (daytime mean pH ~5.2 and nighttime mean pH ~5.6) and remained nearly constant around ~5 up to ~2 km above ground level (AGL). While above ~2 km AGL, the mean pH exhibited a more rapid decrease and became highly acidic (mean pH ~0) at ~3 km AGL. Based on observation of aerosol compositions, Guo et al. (2016) also reported that pH at middle troposphere of 5 km AGL was highly acidic (mean pH ~-0.7) and was about 1.7 unit lower than at surface layer over the northeastern US. These spatial features for pH were closely associated with the spatio-temporal variation in the relative abundance of acidic and alkaline fine particle components and their gaseous counterparts. Here, the acidic fine particle components include total sulfate ($SO4^T$ = H_2SO_4(g) + PM25_SO4), total nitrate ($NO3^T$ = HNO_3(g) + PM25_NO3) and total chloride (Cl^T = HCl(g) + PM25_CL), and the alkaline components include total ammonia (NH_x=NH_3(g)+PM25_NH4) and PM25_OCAT.

Thus, we define the concentrations for total potential anion ($anion^T$) and total potential cation ($cation^T$) as:

$$C_{anion^T} = 2 \cdot C_{SO4^T} + C_{NO3^T} + C_{Cl^T} \quad (4)$$

$$C_{cation^T} = C_{NH_x} + C_{PM25\_NA} + C_{PM25\_K} + 2 \cdot C_{PM25\_MG} + 2 \cdot C_{PM25\_CA} \quad (5)$$

As shown in Fig. 3b-3c, the concentration ratio of $cation^T$ to $anion^T$ slightly changed (consistently decreased with the increasing height in night-time, but firstly decreased and then increased with the increasing height in daytime) below ~2 km AGL, and rapidly decreased above ~ 2 km AGL. NH_x had the predominant mole fraction in the sum of $anion^T$ and $cation^T$ below the lower free troposphere (below ~1 km AGL), but its concentrations decreased sharply with the increasing height (Fig. 3e) as ammonia only had surface emissions. Although also dominated by the surface emission source of SO_2

and NO_x, both $SO4^T$ (= H_2SO_4(g) + PM25_SO4) and $NO3^T$ (= HNO_3(g) + PM25_NO3) could be produced through different gas-phase and aqueous-phase oxidation pathways at different altitudes. Thus, although their concentrations also decreased with the increasing altitude (Fig. 3d), the decreasing rate was slower than that of NH_x (Figs. 3d-3e), which led to an increase in mole fraction of $anion^T$ above ~ 2 km AGL (Figs. 3b-3c). The vertical profile of PM25_OCAT was distinct from that of NH_x (Fig. 3e), with its concentrations remained almost constant until ~1.5 km AGL and relatively slowly decreased above it, suggesting a different source possibly from high-altitude transport. Based on satellite, lidar and surface measurement data, Huang et al. (2008) studied the vertical structure of Asian dust originated from Taklamakan and Gobi deserts, and found that dust particles could be uplifted to an altitude of ~ 9 km around the source region, followed by the efficient eastward transport mainly via westerly jets. Zhang et al. (2018b) also investigated the dust layering structure over some cities in East Asia (including Beijing, Seoul and Tokyo), and indicated that the dust particles were well mixed in the boundary layer before the intensive intermingling of subsiding layers from above (the passage of dust storm). Our simulation also shows that PM25_OCAT over the Beijing site was evenly mixed after a long-range transport from its source region (mainly in Gobi deserts, shown in Fig. S9 of Supplement) below the lower free troposphere. Under different environmental conditions, the changes in concentrations and mole fractions of acidic and alkaline components lead to competition and different dominator factors in the changes of pH vertically. Above ~2km, the influences of acidic components (mainly $SO4^T$ and $NO3^T$) on pH eventually prevailed over those from alkaline components. Interestingly, PM25_OCAT could play a key role in maintaining a less acidic pH at ~1.5-2.0 km AGL. Sensitivity test shows that if the PM25_OCAT is completely removed (in OCAT0 scenario), pH at 2.0 km AGL would be ~ 1 unit lower (more acidic) than that at 1.5 km AGL.

3.3 Diurnal cycle of pH over Beijing

Figure 3a shows that at the Beijing site the night-time pH was slightly higher than the daytime pH below ~1 km AGL, but became lower above ~ 1 km. As shown in Fig. 4, such opposite pattern was largely driven by a different diurnal cycle of aerosol pH at different altitudes. Aerosol pH at surface layer showed a minimum in the early afternoon while at 2 km it showed a maximum around this time (Fig. 4a-4b). The diurnal variation of pH also showed a highly similar pattern as the mole ratio of $cation^T$ to $anion^T$ (Fig. 4a-4b). At surface layer, concentrations of $cation^T$ were considerably higher than concentrations of $anion^T$ (Fig. 4d), furthermore the diurnal variation of NH_x to a large extent explained the diurnal cycle pattern of $cation^T$. Daytime NH_x concentrations were significantly lower than at the night-time, due to a stronger boundary layer mixing. Following Song et al. (2018), we define the concentrations of required NH_x (NH_x^{Req}) as:

$$C_{\mathrm{NH_x^{Req}}} = 2 \cdot C_{\mathrm{SO_4^T}} + C_{\mathrm{NO_3^T}} + C_{\mathrm{Cl^T}} - C_{\mathrm{PM25\_NA}} - C_{\mathrm{PM25\_K}} - 2 \cdot C_{\mathrm{PM25\_MG}} - 2 \cdot C_{\mathrm{PM25\_CA}} \quad (6)$$

The physical meaning for NH_x^{Req} is the minimum NH_x ideally immobilizes all the gas phase H_2SO_4, HNO_3 and HCl. Thus, the concentration ratio of NH_x^{Req} to NH_x describes the levels of ammonia excess (Liu et al., 2017;Song et al., 2018). Diurnal cycle of pH and ammonia excess matched quite well with each other (Fig. 4b), and enhanced ammonia excess corresponded with a higher pH during night-time. PM25_OCAT (mainly originated from long-range transport) concentrations were higher in daytime. $SO4^T$ rapidly accumulated during the night (when the aqueous phase production was active), while $NO3^T$ concentrations reached the peak in the late afternoon (gas phase oxidation played a more important role). As shown in Fig. 4c, a higher aerosol water content during night-time (due to higher RH and $PM_{2.5}$ loading) would also contribute to the less acidic condition. At layer of ~2 km AGL, pH diurnal cycle was also similarly associated with the variation in mole ratio of $cation^T$ to $anion^T$ (peaks around the noon), and the diurnal variation of PM25_OCAT might play an important role.

3.4 pH variabilities over the North China Plain

Figures 5a-5b show that aerosol pH at surface layer exhibited a large spatial variability in the North China Plain. High pH > 6 was found in areas north of ~41°N, which could be attributed to abundant crustal components originated from dust and low concentrations of other aerosol inorganic compositions due to low emissions of precursors (e.g., SO_2, NO_x and NH_3). In areas south of ~41°N, mean aerosol pH fell mostly between 4.4 and 5.7 (10% and 90% quantiles, respectively) with less contribution of crustal components. Mean pH over the sea mainly ranged between 4.0 and 4.5, generally lower than over the most terrestrial areas. These marine and terrestrial areas with a relatively more acidic aerosol phase (pH ~4.0 to 5.0) corresponded well with the spatial distribution of low NH_x zones (Fig. 5d). Besides, a large temporal variability of pH was also found at the surface layer (Fig. 5c). The simulated standard deviation of pH mostly ranged between 0.4 and 2 and was higher over the northern areas with episodic dust events, as well as the southern areas with lower NH_x emissions.

Figure 6a shows the latitude-height cross section of aerosol pH in the North China Plain. The trend that aerosol acidity was enhanced with the increasing altitudes was consistent for all the latitudes investigated. Nonetheless, the vertical gradients of pH varied among different locations, closely associated with the vertical profile of the relative abundance of $cation^T$ and $anion^T$, as well as air temperature and humidity (Fig. S10 of Supplement). Figure 6b further compares the vertical profiles of aerosol pH over seven different cities in the North China Plain (locations shown in Fig. 5c). The vertical profile pattern of aerosol pH was highly similar among Beijing, Tianjin, Baoding and Shijiazhuang, wherein the pH changed slightly until above ~ 2 km AGL. However, as shown in Fig. 5c and Fig. S10, pH decreased rapidly from 1 to 2 km AGL over both Zhangjiakou and Taiyuan, maybe due to the lack of alkaline fine particle components (NH_x or PM25_OCAT). Rapid production of sulfate and nitrate at 0.5-1 km AGL over Jinan was observed (Fig. S10), leading to a lower pH there. Furthermore, monthly mean night-time pH was mostly higher than daytime pH in the lowest boundary layer below ~100

m AGL, however no consistent pattern was found for the diurnal cycle pattern of pH in the upper tropospheric layers (Fig. 6c).

3.5 Regime transition of sulfate formation

Figure 7a shows the averaged contribution of six sulfate formation pathways, namely aerosol water phase oxidation by dissolved O_3, NO_2, H_2O_2, TMI (in the presence of O_2) and CH_3OOH, as well as gas-particle partitioning of H_2SO_4 vapor (GPP) at the surface layer. Note that H_2SO_4 vapor is produced mainly from the oxidation of SO_2 by OH radical, and then partitions almost completely into the aerosol phase. For areas north of 41°N, oxidation by dissolved O_3 was the most important pathway, followed by TMI pathway. To the south of 41°N, NO_2, TMI and H_2O_2 pathways played the dominant role. The NO_2 reaction pathway prevailed in the megacity region of Beijing and the large area of Hebei Province to the south and west of Beijing, as well as part of Shandong Province, while the TMI pathway dominated in the inland region to the west and the coastal regions to the east of Beijing, and the H_2O_2 pathway dominated in the region further south in Shandong and Henan provinces. The regime transition of sulfate formation pathways highly depended on the spatial distribution of pH and oxidants/catalysts. As shown in Fig. 7b-7e, spatial distribution for O_3 exhibited an opposite pattern as NO_x, i.e., O_3 concentrations in urbanized areas (e.g., Beijing) with high NO_x emissions were considerably lower than less industrialized areas, due to the titration effects of NO.

Figure 8b shows the vertical profile of sulfate production rates averaged over the four dominant sulfate formation regimes at the surface layer (i.e., O_3, NO_2, TMI and H_2O_2, shown in Fig. 8a). Consistent with the surface layer, the vertical regime transition of sulfate formation highly depended on the vertical distribution of pH and oxidants/catalysts (Fig. 8c-8f). Both O_3 and TMI pathways played the dominant role at higher altitudes between 0.5-2.0 km AGL (Fig. 8b). Interestingly, the vertical profile pattern for pH potentially enhanced TMI pathway but hindered O_3 pathway, while the vertical profile pattern for concentrations of oxidants/catalysts disfavored TMI pathway but favored O_3 pathway. As shown in Fig. 8b, the relative contributions of NO_2 pathway rapidly decreased with the increasing altitudes, consistent with the decreasing trend in both NO_2 concentrations (Fig. 8f) and aerosol pH. H_2O_2 pathway was non-negligible only in the lower boundary layer over the H_2O_2-regime and NO_2-regime. GPP pathway tended to become more important with the increasing altitudes, mainly due to the decreasing trend in aerosol water content. At higher altitudes above ~3 km AGL, aqueous phase oxidation in aerosol water became negligible.

Compared to nitrate, aqueous phase oxidation was more important to sulfate formation in North China Plain. For example, according to our simulation, over the Beijing site, below ~2 km AGL, aqueous phase oxidation in aerosol water accounted

for the ~100% and 80-90% of $SO4^T$ formation during night-time and daytime, respectively. While, its respective contributions to night-time and daytime $NO3^T$ formation were only 40-70% and 0-10%.

3.6 Discussion

The uncertainties of predicted pH and sulfate formation relevant to the adjusted emission parameters (for NH_3, crustal minerals, Fe^{3+}/Mn^{2+} ions and chlorides) and assumed phase state are further investigated. We focus on 4 aspects, namely surface layer pH (denoted as pH_{surf}) and its day/night difference (denoted as $\Delta pH_{surf,night-day}$), the difference between surface layer pH and pH at ~2 km AGL (denoted as $\Delta pH_{surf-2km}$), and surface layer sulfate production rates (denoted as $P_{S(VI),surf}$) through different pathways for the domain-wide grid cells south of 41°N. As shown in Fig. 9, different scenarios predict different pH_{surf} and $P_{S(VI),surf}$, nonetheless $\Delta pH_{surf,night-day}$ and $\Delta pH_{surf-2km}$ is approximately 0.2 and 5.0, respectively for almost all the sensitivity tests, indicating that the diurnal cycle pattern at surface layer and the altitudinal decrease in pH shall be robust.

We first examine the sensitivities of our results to NH_3 and crustal minerals. When NH_3 emissions are completely removed (A0 scenario), a strong acidic aerosol phase is predicted (mean pH_{surf} ~0), meanwhile the $P_{S(VI),surf}$ decreases by ~60% as in CTRL scenario (due to lack of efficient water-absorbing ammoniates). If PM25_OCAT emissions are removed or halved (OCAT0 and OCAT0.5 scenarios), averaged pH decreases to 4.2 and 4.6, respectively, and $P_{S(VI),surf}$ increases by ~250% and ~200%, respectively, compared to the CTRL scenario (a lower pH favors sulfate production through TMI pathway). Doubling both NH_3 and PM25_OCAT emissions (A2 and OCAT2 scenarios) leads to a slightly higher pH_{surf} and a similar $P_{S(VI),surf}$, with the sulfate formation dominated by NO_2 and O_3 pathways. For the control experiments of MEIC_CTRL (using the original MEIC inventory), predicted pH_{surf} is lower, and the relative contribution to sulfate formation is decreased for NO_2 pathway but increased for TMI pathway. Interestingly, rapid production of sulfate could be maintained over a wide pH range (~4.2-5.7) with the varying emissions Interestingly, rapid production of sulfate could be maintained over a wide pH range (~4.2-5.7) with the varying emissions Interestingly, rapid production of sulfate could be maintained over a wide pH range (~4.2-5.7) with the varying emissions Interestingly, rapid production of sulfate could be maintained over a wide pH range (~4.2-5.7) with the varying emissions for NH_3 and crustal particles (transition between TMI pathway dominated and NO_2/O_3 pathway dominated).

We have also investigated the effect of emissions of chlorides and Fe^{3+}/Mn^{2+} ions. Removing all the chloride emissions (CL0 scenario) has a negligible effect on both aerosol pH and sulfate production. However, if the chloride emissions are

doubled (CL2 scenario), pH slightly decreases to 5.0, and $P_{S(VI),surf}$ increases by 50% (maybe increase in NH_4Cl leading to an enhanced water absorption). When both FS_{FE3+} and FS_{MN2+} equal to zero (TMI0 scenario, and TMI pathway is shut down), $P_{S(VI),surf}$ decrease almost by half and pH_{surf} (5.5) is slightly higher. Interestingly, when both FS_{FE3+} and FS_{MN2+} are halved (TMI0.5 scenario), a similar pH_{surf} and $P_{S(VI),surf}$ is predicted as in TMI0 scenario. When both FS_{FE3+} and FS_{MN2+} are doubled (TMI2 scenario), $P_{S(VI),surf}$ increase by ~300% and pH_{surf} decreases to 4.6. Our results indicate that sulfate production is rather sensitive to the availability of TMI species. Unfortunately, the concentrations as well as sources for TMI species in aerosol water during haze episodes remain not well constrained and understood. The simulated mean concentration for Fe^{3+} and Mn^{2+} in $PM_{2.5}$ at the Beijing TSU site is 3.2 and 3.6 ng/m^3, respectively, and are smaller than the observed concentrations for soluble Fe and Mn (1.5-16 and 10-41 ng/m^3, respectively) in $PM_{2.5}$ at a Xi'an site (Wang et al., 2016). Note that Fe^{3+}/Mn^{2+} ions also have an anthropogenic source, and were estimated to account for 10-30% in Beijing (Shao et al., 2019). Fe^{3+}/Mn^{2+} ions also have an anthropogenic source, and were estimated to account for 10-30% in Beijing (Shao et al., 2019). Furthermore, the soluble Fe/Mn speciation (including Fe^{3+}-Fe^{2+}, Mn^{2+}-Mn^{3+}-Mn^{4+} cycling) depends on dust mineralogy, particle acidity and heterogeneous redox reactions (Takahashi et al., 2011;Schroth et al., 2009), and is very difficult to be explicitly treated. Also the activity coefficients for Fe^{3+}/Mn^{2+} ions under the high ionic strength environment might differ (Cheng et al., 2016). The treatment of TMI pathway should be further improved in future studies.

设置了格式: 上标

设置了格式: 上标

设置了格式: 下标

设置了格式: 上标

Different phase state assumptions predict slightly different pH_{surf}, but distinct sulfate production. Compared with CTRL scenario, assuming a fixed metastable phase state (MSTB scenario) predicts a slightly lower pH_{surf} (5.0) and 40% higher $P_{S(VI),surf}$, and the contribution of TMI pathway increases. Assuming a fixed stable phase state predicts a slightly higher pH (5.3) and 25% lower $P_{S(VI),surf}$ (maybe mainly due to the changes in predicted aerosol water content), and the contribution of NO_2 pathway increases. Previous box model studies reported a similar finding regarding the minor impacts of phase state assumption on pH (Song et al., 2018).

4. Conclusions

The focus of the current study is to investigate the spatio-temporal variabilities of aerosol pH and regime transitions of sulfate formation at a regional scale. For this purpose, an aqueous phase chemistry module (AWAC) for sulfate and nitrate formation in aerosol water has been developed and implemented, using the results (including aerosol water and pH) of revised ISORROPIA II model as input data. With this improved version of Weather Research Forecasting Model with Chemistry (WRF−Chem), we simulated the severe and successive haze pollution spreading over the North China Plain

during January of 2013. Control experiments could well reproduce the observed inorganic components of fine particles (including sulfate, nitrate, ammonium, chloride, sodium, and crustal minerals), as well as SO_2, NO_2, O_3 and relative humidity, compared to the observations at the Beijing Tsinghua University site. Impacts of the uncertainties in parameters and assumptions have also been discussed.

The vertical profile and diurnal cycle pattern for aerosol pH were closely associated with the spatio-temporal variation in the relative abundance of acidic and alkaline fine particle components and their gaseous counterparts. The competition between the ammonia, crustal particles and acidic components (such as sulfate and nitrate) could play an important role in determining pH in different vertical layers. The monthly mean pH at surface layer exhibited a large spatial variability over the North China Plain. Mean pH was greater than 6 for the areas with higher latitudes north of 41°N (mainly influenced by the abundant crustal particles) and was mostly within 4.4 and 5.7 (10% and 90% quantiles, respectively) for vast areas south of ~41°N (with NH_x as the driving factor) over the North China Plain. The trend that aerosol acidity was enhanced with the increasing altitudes was consistent for all latitudes (35-43°N) investigated, while the vertical gradients of pH varied between different locations. The diurnal cycle pattern existed only for the domain-wide cells in the lower boundary layer, wherein night-time pH was higher.

In the AWAC module, six sulfate formation pathways in aerosol water are implemented and compared, namely aqueous phase oxidation by dissolved O_3, NO_2, H_2O_2, TMI (in the presence of O_2) and CH_3OOH, as well as gas-particle partitioning of H_2SO_4 vapor (GPP). The relative contributions of different sulfate formation pathways in aerosol water depended on both pH as well as the concentrations of each oxidant/catalyst. At surface layer, O_3, NO_2, TMI and H_2O_2 pathways were the most important in different locations over the North China Plain, and four regions with three distinct regimes have been found. With the increasing height, O_3, TMI and GPP pathways became more important, while contributions from NO_2 and H_2O_2 pathways decreased rapidly. At higher altitudes above ~3 km above ground level, aqueous phase oxidation in aerosol water became negligible.

The diurnal cycle pattern at surface layer and altitudinal decrease for pH is consistent for all the sensitivity tests with varying adjusted emission parameters and phase state assumptions except when NH_3 emissions are completely removed. pH is sensitive to the alkalization effect of NH_3 and crustal particles, furthermore, rapid production of sulfate could be maintained over a wide pH range (e.g., 4.2-5.7) with the varying emissions for NH_3 and crustal particles (transition from TMI pathway dominated to NO_2/O_3 pathway dominated). The sulfate production is rather sensitive to the concentrations of TMI species and doubling the TMI species sources almost triples the sulfate production. Changes in chloride emissions as well as phase state assumptions both have a relatively minor effect on pH, but sulfate formation could be changed as the predicted aerosol water changes. Our studies suggest that sources of crustal particles, NH_3 and TMI

species are very important factors for the aqueous phase chemistry during haze episodes and should be better constrained in future studies. Moreover, the use of a more detailed aqueous phase mechanism involving the TMI species cycling and radical chain propagation is suggested. Uncertainties relevant with the algorithms to solve the aerosol thermodynamics, including the treatment of non-ideality, size effects, phase state, mixing state, the interactions between inorganic compounds and organic compounds, as well as phase separation, should also be addressed in future studies.

Acknowledgements

Acknowledgements

This study is supported by Max Planck Society (MPG). Y. Cheng would like to thank the Minerva program of MPG.

Author contribution: H.S. and Y.C. designed and led the study. W.T. developed the AWAC module and implemented the revised ISORROPIA II into WRF-Chem. W.T. performed model simulations. W.T., H.S. and Y.C. analyzed data and interpreted the results. G.Z. supported the data analyses. J.W., C.W. and L.L. supported modeling work. M.L. and Q.Z. provided the MEIC for the year of 2013. All coauthors have discussed results and commented on the manuscript. W.T. wrote the manuscript with input from all coauthors.

Figures

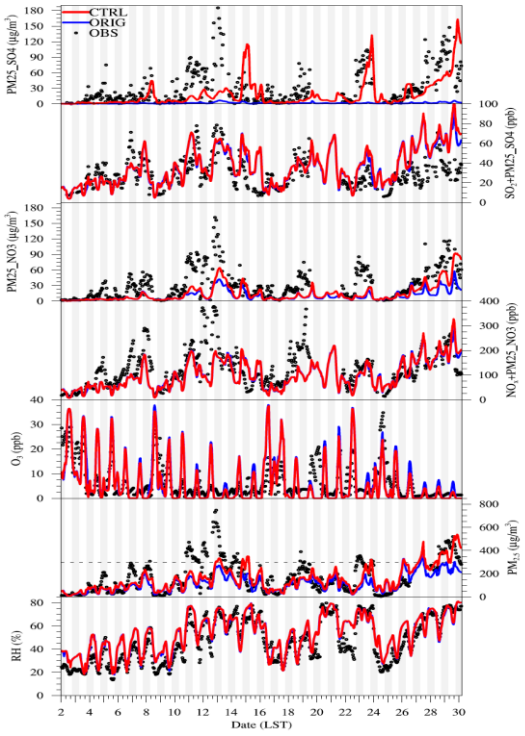

Figure 1. Comparison of hourly model results and observations (OBS) for ORIG and CTRL scenarios at Beijing TSU site during January 2013. The compared parameters include modelled hourly concentrations of fine particulate sulfate (PM25_SO4), the sum of SO_2 and PM25_SO4 (PM25_SO4 converted to the equivalent volume mixing ratio of SO_2), fine particulate nitrate (PM25_NO3), the sum of NO_x and PM25_NO3 (PM25_ NO3 converted to the equivalent volume mixing ratio of NO_x), O_3 and $PM_{2.5}$, as well as hourly relative humidity (RH).

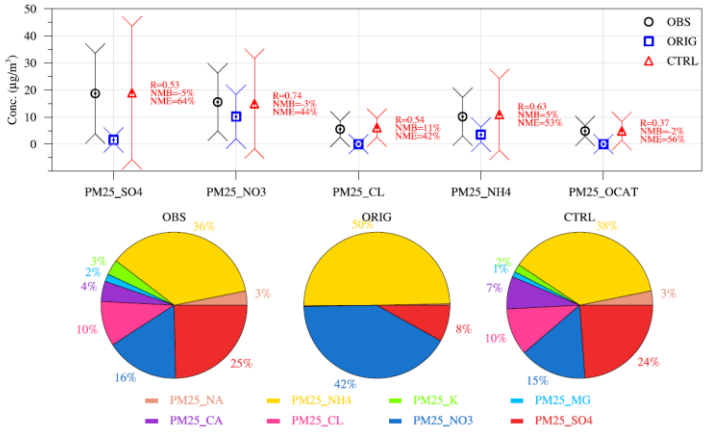

Figure 2. Significant improvement of simulations in the CTRL scenario compared with that in the ORIG scenario. Bottom panel: observed (OBS) and simulated (scenarios of ORIG and CTRL) mean electric charge fractions for fine particulate sulfate (PM25_SO4, using SO_4^{2-} as the surrogate), nitrate (PM25_NO3), ammonium (PM25_NH4), chloride (PM25_CL), sodium (PM25_NA), potassium (PM25_K), calcium (PM25_CA) and magnesium (PM25_MG) at Beijing TSU site during January of 2013. Top panel: observed (OBS) and simulated (scenarios of ORIG and CTRL) concentrations (both average and standard deviation are shown) for fine particulate sulfate (PM25_SO4), nitrate (PM25_NO3), chloride (PM25_CL), ammonium (PM25_NH4) and other cation components (PM25_OCAT=PM25_NA+PM25_K+PM25_CA+PM25_MG) at Beijing TSU site during January of 2013.

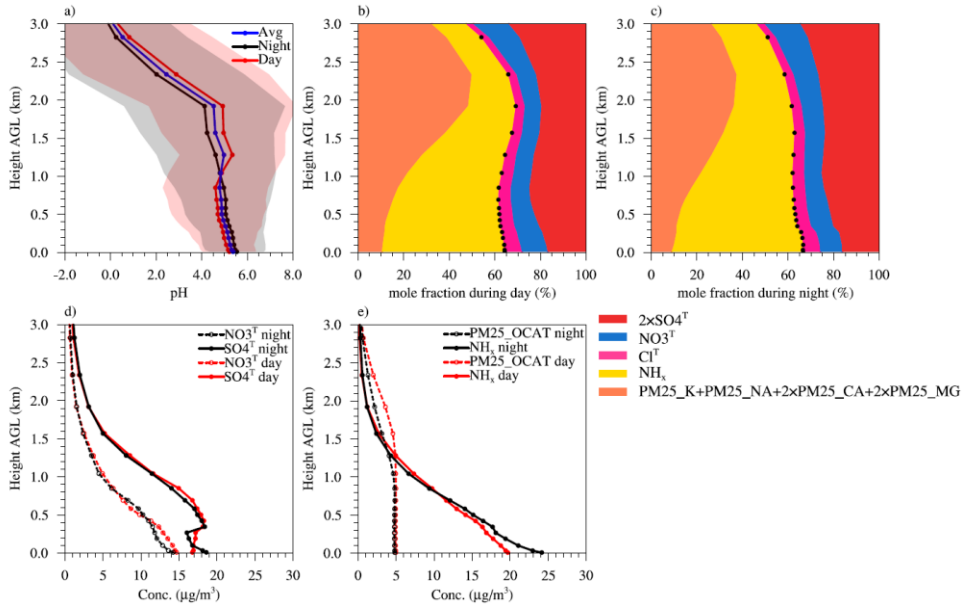

Figure 3. Vertical profiles of the fine particle pH and its potential influencing factors over Beijing TSU site. The data are simulated with the CTRL scenario during January of 2013 and presented at height above ground level (AGL). (a) Monthly average pH (blue), as well as daytime (red) and night-time (black) average pH (standard deviations are shown as light grey and light red shadings, respectively). (b) Daytime mole fractions for the electric charge of total ammonia (NH_x), total chloride (Cl^T), total sulfate ($SO4^T$), total nitrate ($NO3^T$) and different crustal components of $PM_{2.5}$, and the black dots represent the vertical profile of $cation^T/(cation^T+anion^T)$. (c) The same as in (b), but for the night-time. (d) Daytime (red) and night-time (black) concentrations of total sulfate ($SO4^T$) and total nitrate ($NO3^T$). (e) Daytime (red) and night-time (black) concentrations of NH_x and PM25_OCAT.

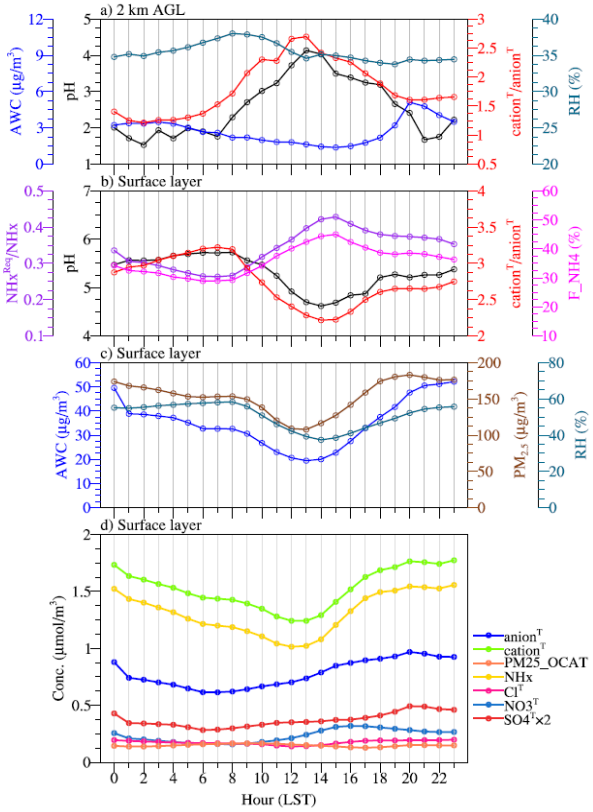

Figure 4. Monthly mean diurnal cycle for (a) fine particle pH, aerosol liquid water content (AWC), the mole ratio of total potential cation ($cation^T$) to total potential anion ($anion^T$), and relative humidity (RH) at 2 km AGL, (b) fine particle pH, the mole ratio of $cation^T$ to $anion^T$, the mole ratio of required NH_x (NH_x^{Req}) to NH_x, fraction of NH_x in the particle phase (F_NH4) at surface layer, (c) AWC, RH and $PM_{2.5}$ concentrations at surface layer, (d) concentrations for total sulfate ($SO4^T$), total nitrate ($NO3^T$), total chloride (Cl^T), total ammonia (NH_x), PM25_OCAT, $cation^T$ and $anion^T$ at surface layer simulated in CTRL scenario at Beijing TSU site during January of 2013.

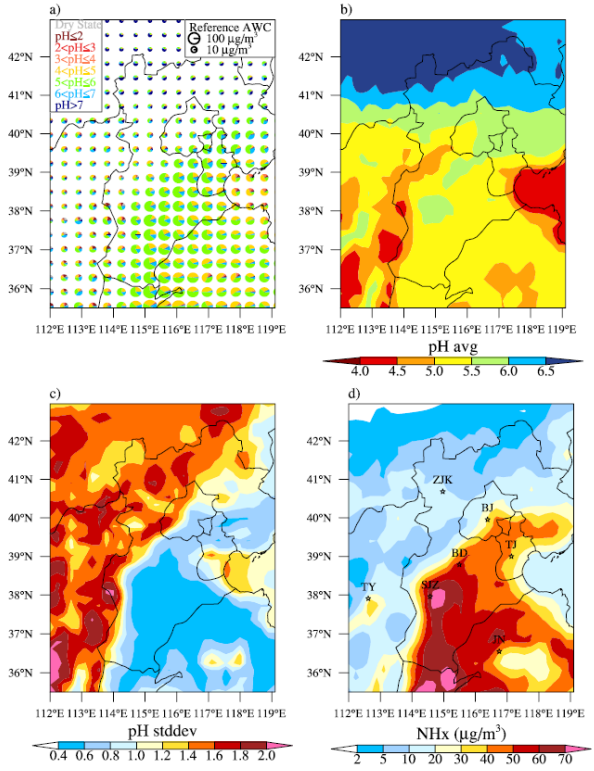

Figure 5. Fine particle pH and NH_x concentrations at surface layer simulated in CTRL scenario during January of 2013: a) the frequencies for different pH ranges (the radius R for the pie chart is scaled using $R/R_{ref}=2\exp(\log10(AWC/AWC_{ref}))$, and the reference radius R_{ref} and aerosol liquid water content (AWC_{ref}) are also shown), horizontal distribution of the average (b) as well as standard deviation (c) for pH and the concentrations for NH_x (d). The locations for the 7 cities of Beijing (BJ), Tianjin (TJ), Zhangjiakou (ZJK), Baoding (BD), Shijiazhuang (SJZ), Taiyuan (TY) and Jinan (JN) are also shown.

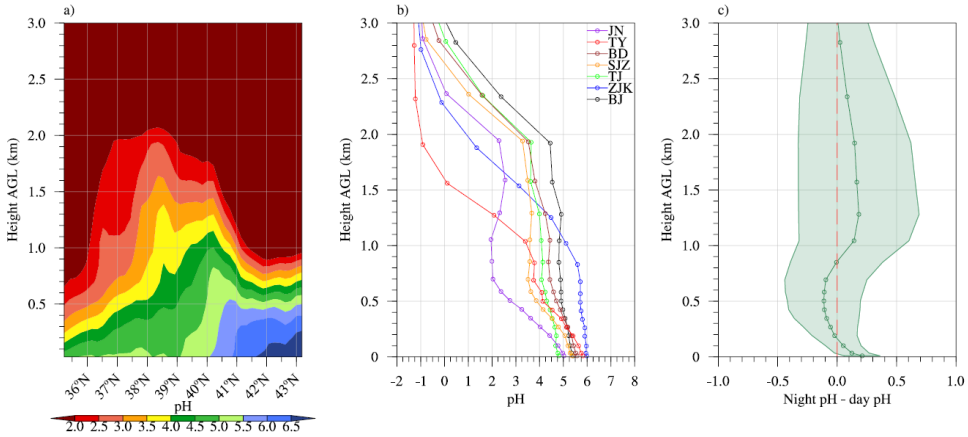

Figure 6. (a) Latitude-height cross section for the monthly mean fine particle pH averaged between 113-119°E, (b) vertical profile for the monthly mean fine particle pH over the 7 cities of Beijing (BJ), Tianjin (TJ), Zhangjiakou (ZJK), Baoding (BD), Shijiazhuang (SJZ), Taiyuan (TY) and Jinan (JN) (locations shown in Fig. 5c), (c) vertical profile for the monthly mean day-night difference of pH (standard deviation is shown as shading) for the domain-wide grid cells in CTRL scenario during January of 2013.

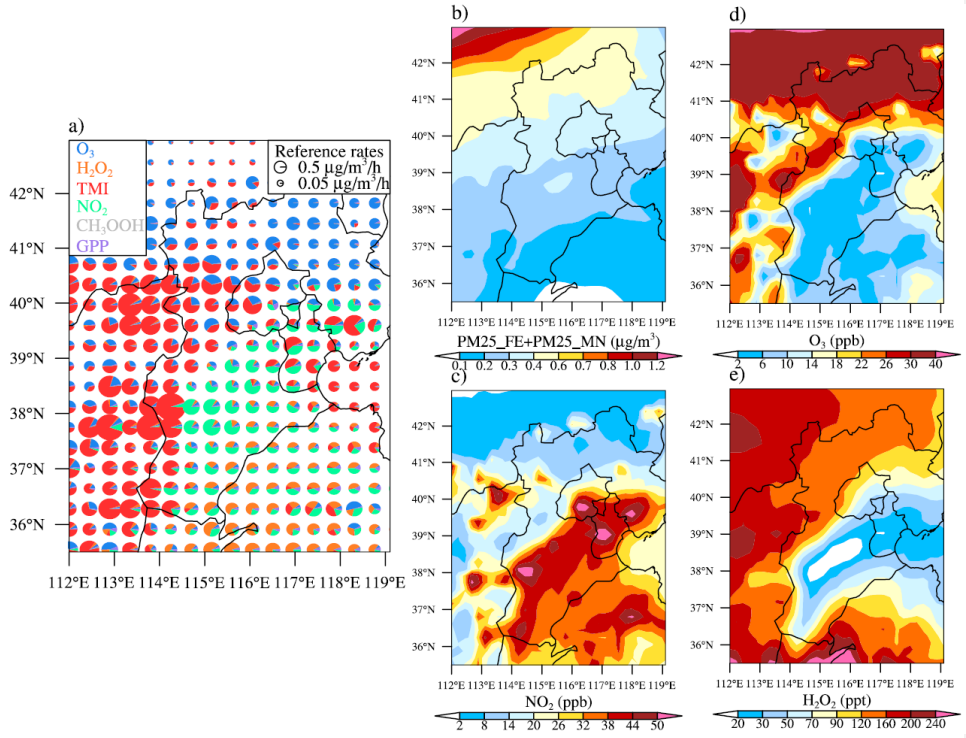

Figure 7. (a) The relative contributions of six sulfate formation pathways, namely aqueous phase oxidation by dissolved O_3, H_2O_2, TMI (in presence of O_2), NO_2 and CH_3OOH, as well as gas-particle partitioning of H_2SO_4 vapour (GPP) at surface layer simulated in CTRL scenario during January of 2013. The radius R for the pie chart in the top panel is scaled using $R/R_{ref}=2\exp(\log10(P/P_{ref}))$, and the reference sulfate production rate P are also shown. Horizontal distribution for the concentrations of (b) the sum of PM25_FE and PM25_MN, (c) NO_2, (d) O_3 as well as (e) H_2O_2 simulated in CTRL scenario during January of 2013.

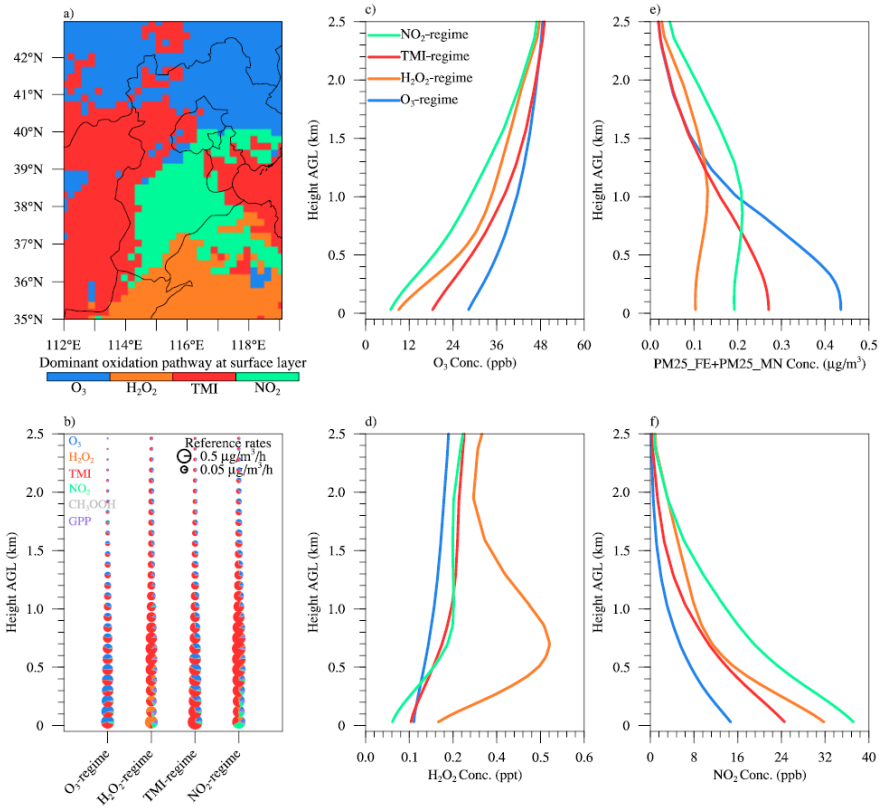

Figure 8. Dominant sulfate formation pathway at surface layer (a), the vertical profile of sulfate production through different pathways (b), as well as concentrations for the oxidants of O_3 (c), H_2O_2 (d), TMI (e) and NO_2 (f), respectively averaged over the four dominant oxidation regimes (O_3, H_2O_2, TMI and NO_2, respectively, as shown in Fig. 8a) simulated in CTRL scenario during January of 2013. Contributions from different sulfate formation pathways are also shown in pie charts, and the radius R for pie chart is scaled depending on sulfate production rate P using $R/R_{ref}=2\exp(\log10(P/P_{ref}))$.

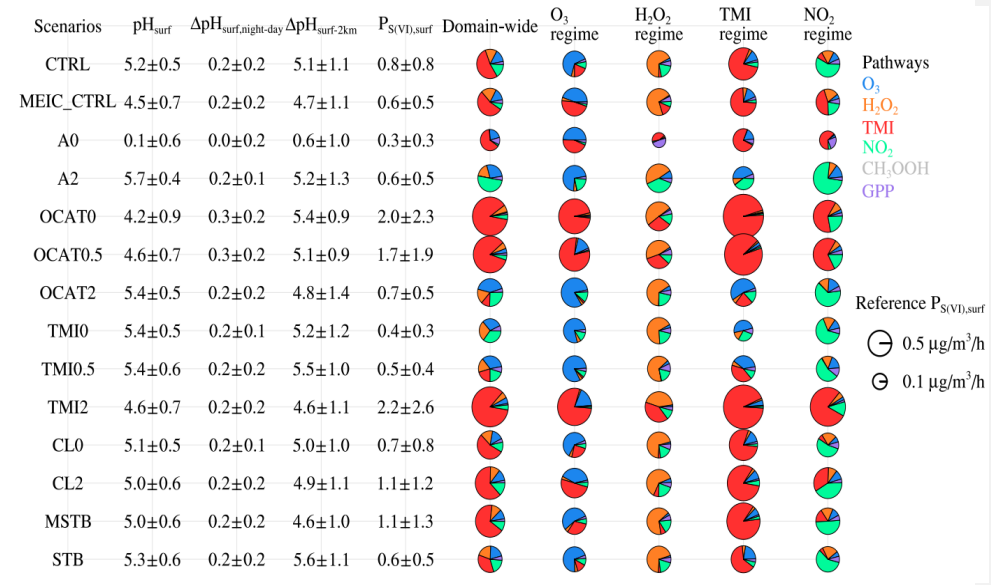

Figure 9. Surface layer pH (denoted as pH_{surf}) and its day-night difference (denoted as $\Delta pH_{surf,night-day}$), the difference between surface layer pH and pH at ~2 km AGL (denoted as $\Delta pH_{surf-2km}$), and surface layer sulfate production rates (denoted as $P_{S(VI),surf}$) for the domain-wide grid cells south of 41°N in control experiment and sensitivity experiments during January of 2013. Contributions from different sulfate formation pathways over the domain-wide grid cells south of 41°N and the four dominant sulfate formation regimes (O_3, H_2O_2, TMI and NO_2, respectively, as defined in Fig. 8a) are also shown in pie charts. The radius R for pie chart is scaled depending on sulfate production rate P using $R/R_{ref}=2\exp(\log10(P/P_{ref}))$.

Tables

Table 1. Rate expressions and rate constants for the S(IV) oxidation reactions in the aerosol water.

Oxidants	Rate expression ($M\ s^{-1}$)	References
O_3	$r_{O_3+S(IV)} = (k_0[SO_2 \cdot H_2O] + k_1[HSO_3^-] + k_2[SO_3^{2-}])[O_3(aq)]$ k_0=2.4×10^4 $M^{-1}s^{-1}$ k_1=3.7×10^5 $M^{-1}s^{-1}$, E/R=5530 K k_2=1.5×10^9 $M^{-1}s^{-1}$, E/R=5280 K	Seinfeld and Pandis (2016)
H_2O_2	$r_{H_2O_2+S(IV)} = (k_3[H^+][HSO_3^-][H_2O_2(aq)]) / (1+13\cdot[H^+])$ k_3=7.45×10^7 $M^{-1}s^{-1}$, E/R=4430 K	Seinfeld and Pandis (2016)
TMI	$r_{TMI+S(IV)} = \begin{cases} k_4[H^+]^{-0.74}[Mn^{2+}][Fe^{3+}][S(IV)] & pH \le 4.2 \\ k_5[H^+]^{0.67}[Mn^{2+}][Fe^{3+}][S(IV)] & pH > 4.2 \end{cases}$ k_4=3.72×10^7 $M^{-1.26}s^{-1}$ k_5=2.51×10^{13} $M^{-2.67}s^{-1}$	Ibusuki and Takeuchi (1987) Cheng et al. (2016)
NO_2[a]	$r_{NO_2+S(IV)} = k_6[NO_2(aq)][S(IV)]$ lower estimate: $k_{6,low}$=(0.14~2)×10^6 $M^{-1}s^{-1}$ higher estimate: $k_{6,high}$=(1.24~1.67)×10^7 $M^{-1}s^{-1}$ k_6 is the average of $k_{6,low}$ and $k_{6,high}$	Seinfeld and Pandis (2016) Lee and Schwartz (1983) Clifton et al. (1988) Cheng et al. (2016)
CH_3OOH	$r_{CH_3OOH+S(IV)} = k_7[H^+][HSO_3^-][CH_3OOH]$ k_7=1.75×10^7 $M^{-2}s^{-1}$, E/R=3801 K	Walcek and Taylor (1986)

[a] The rate coefficient k_6 (with a unit of $M^{-1}s^{-1}$) is expressed as:

$$k_6 = \begin{cases} (k_{6,low,1} + k_{6,high,1})/2 & pH \le 5 \\ (k_{6,low,1} + (pH-5)/0.8\times(k_{6,low,2} - k_{6,low,1}) + k_{6,high,1})/2 & 5<pH\le 5.3 \\ (k_{6,low,1} + (pH-5)/0.8\times(k_{6,low,2} - k_{6,low,1}) + k_{6,high,1} + (pH-5.3)/3.4\times(k_{6,high,2} - k_{6,high,1}))/2 & 5.3<pH\le 5.8 \\ (k_{6,low,2} + (pH-5.3)/3.4\times(k_{6,high,2} - k_{6,high,1}))/2 & 5.8<pH\le 8.7 \\ (k_{6,low,2} + k_{6,high,2})/2 & pH>8.7 \end{cases}$$

where $k_{6,low,1}=0.14\times10^{6}\ M^{-1}s^{-1}$, $k_{6,low,2}=2\times10^{6}\ M^{-1}s^{-1}$, $k_{6,high,1}=1.24\times10^{7}\ M^{-1}s^{-1}$, $k_{6,high,2}=1.67\times10^{7}\ M^{-1}s^{-1}$

Table 2. Description for different scenarios in this study.

Number	Name	Description
1	ORIG	*emissf*$_{NH3}$=1, *emissf*$_{OCAT}$=0, *emissf*$_{CL}$=0, and aqueous phase oxidation in the aerosol water is excluded.
2	CTRL	Control experiment tuned to match the observations at Beijing TSU site. A fixed metastable (stable) phase state is assumed if RH is greater (not greater) than 30%. *emissf*$_{NH3}$=2, *emissf*$_{OCAT}$=4.5, *emissf*$_{CL}$=6, *FS*$_{Fe3+}$=7% and *FS*$_{Mn2+}$=40%.
3	MEIC_CTRL	The same as CTRL, except *emissf*$_{NH3}$=1 (original MEIC inventory), *FS*$_{Fe3+}$=0.35% and *FS*$_{Mn2+}$=20%. Another control experiment tuned to match the observations at Beijing TSU site.
4-5	A0, A2	The same as CTRL, except *emissf*$_{NH3}$ is set to zero, halved and doubled, respectively.
6-7	OCAT0, OCAT0.5, OCAT2	The same as CTRL, except *emissf*$_{OCAT}$ is set to zero, halved, halved and doubled, respectively.
9-11	TMI0, TMI0.5, TMI2	The same as CTRL, except *FS*$_{FE3+}$ and *FS*$_{MN2+}$ are set to zero, halved, halved and doubled, respectively.
12-13	CL0, CL2	The same as CTRL, except *emissf*$_{CL}$ is set to zero, halved and doubled, respectively.
14-15	MSTB, STB	The same as CTRL, except a fixed metastable/stable phase state is assumed.

References

Ackermann, I. J., Hass, H., Memmesheimer, M., Ebel, A., Binkowski, F. S., and Shankar, U.: Modal aerosol dynamics model for Europe: Development and first applications, Atmospheric Environment, 32, 2981-2999, 1998.

Baker, A. R., Jickells, T. D., Witt, M., and Linge, K. L.: Trends in the solubility of iron, aluminium, manganese and phosphorus in aerosol collected over the Atlantic Ocean, Marine Chemistry, 98, 43-58, 10.1016/j.marchem.2005.06.004, 2006.

Brimblecombe, P.: The Big Smoke (Routledge Revivals): A History of Air Pollution in London Since Medieval Times, Routledge, 2012.

Chen, D., Liu, Z., Fast, J., and Ban, J.: Simulations of sulfate–nitrate–ammonium (SNA) aerosols during the extreme haze events over northern China in October 2014, Atmos. Chem. Phys., 16, 10707-10724, 2016.

Chen, T., Chu, B., Ge, Y., Zhang, S., Ma, Q., He, H., and Li, S. M.: Enhancement of aqueous sulfate formation by the coexistence of NO2/NH3 under high ionic strengths in aerosol water, Environ Pollut, 252, 236-244, 10.1016/j.envpol.2019.05.119, 2019.

Cheng, Y., Zheng, G., Wei, C., Mu, Q., Zheng, B., Wang, Z., Gao, M., Zhang, Q., He, K., Carmichael, G., Poschl, U., and Su, H.: Reactive nitrogen chemistry in aerosol water as a source of sulfate during haze events in China, Sci Adv, 2, e1601530, 10.1126/sciadv.1601530, 2016.

Claquin, T., Schulz, M., and Balkanski, Y. J.: Modeling the mineralogy of atmospheric dust sources, J Geophys Res-Atmos, 104, 22243-22256, Doi 10.1029/1999jd900416, 1999.

Clifton, C. L., Altstein, N., and Huie, R. E.: Rate constant for the reaction of nitrogen dioxide with sulfur(IV) over the pH range 5.3-13, Environ Sci Technol, 22, 586-589, 10.1021/es00170a018, 1988.

Damian, V., Sandu, A., Damian, M., Potra, F., and Carmichael, G. R.: The kinetic preprocessor KPP-a software environment for solving chemical kinetics, Computers & Chemical Engineering, 26, 1567-1579, 2002.

Ding, J., Zhao, P. S., Su, J., Dong, Q., Du, X., and Zhang, Y. F.: Aerosol pH and its driving factors in Beijing, Atmos. Chem. Phys., 19, 7939-7954, 10.5194/acp-19-7939-2019, 2019.

Dong, X. Y., Fu, J. S., Huang, K., Tong, D., and Zhuang, G. S.: Model development of dust emission and heterogeneous chemistry within the Community Multiscale Air Quality modeling system and its application over East Asia, Atmos. Chem. Phys., 16, 8157-8180, 10.5194/acp-16-8157-2016, 2016.

Dufour, G., Eremenko, M., Orphal, J., and Flaud, J. M.: IASI observations of seasonal and day-to-day variations of tropospheric ozone over three highly populated areas of China: Beijing, Shanghai, and Hong Kong, Atmos. Chem. Phys., 10, 3787-3801, DOI 10.5194/acp-10-3787-2010, 2010.

Duvall, R. M., Majestic, B. J., Shafer, M. M., Chuang, P. Y., Simoneit, B. R. T., and Schauer, J. J.: The water-soluble fraction of carbon, sulfur, and crustal elements in Asian aerosols and Asian soils, Atmos. Environ., 42, 5872-5884, 10.1016/j.atmosenv.2008.03.028, 2008.

Fountoukis, C., and Nenes, A.: ISORROPIA II: a computationally efficient thermodynamic equilibrium model for K+–Ca 2+–Mg 2+–NH 4+–Na+–SO 4 2−–NO 3−–Cl−–H 2 O aerosols, Atmospheric Chemistry and Physics, 7, 4639-4659, 2007.

Gen, M. S., Zhang, R. F., Huang, D. D., Li, Y. J., and Chan, C. K.: Heterogeneous Oxidation of SO2 in Sulfate Production during Nitrate Photolysis at 300 nm: Effect of pH, Relative Humidity, Irradiation Intensity, and the Presence of Organic Compounds, Environ. Sci. Technol., 53, 8757-8766, 10.1021/acs.est.9b01623, 2019.

Ginoux, P., Chin, M., Tegen, I., Prospero, J. M., Holben, B., Dubovik, O., and Lin, S. J.: Sources and distributions of dust aerosols simulated with the GOCART model, J Geophys Res-Atmos, 106, 20255-20273, Doi 10.1029/2000jd000053, 2001.

Grell, G. A., Peckham, S. E., Schmitz, R., McKeen, S. A., Frost, G., Skamarock, W. C., and Eder, B.: Fully coupled "online" chemistry within the WRF model, Atmospheric Environment, 39, 6957-6975, 10.1016/j.atmosenv.2005.04.027, 2005.

Guenther, A., Karl, T., Harley, P., Wiedinmyer, C., Palmer, P., and Geron, C.: Estimates of global terrestrial isoprene emissions using MEGAN (Model of Emissions of Gases and Aerosols from Nature), Atmospheric Chemistry and Physics, 6, 3181-3210, 2006.

Guo, H., Sullivan, A. P., Campuzano-Jost, P., Schroder, J. C., Lopez-Hilfiker, F. D., Dibb, J. E., Jimenez, J. L., Thornton, J. A., Brown, S. S., Nenes, A., and Weber, R. J.: Fine particle pH and the partitioning of nitric acid during winter in the northeastern United States, J Geophys Res-Atmos, 121, 10355-10376, 10.1002/2016jd025311, 2016.

Hsu, S. C., Wong, G. T. F., Gong, G. C., Shiah, F. K., Huang, Y. T., Kao, S. J., Tsai, F. J., Lung, S. C. C., Lin, F. J., Lin, I. I., Hung, C. C., and Tseng, C. M.: Sources, solubility, and dry deposition of aerosol trace elements over the East China Sea, Marine Chemistry, 120, 116-127, 10.1016/j.marchem.2008.10.003, 2010.

Huang, J., Minnis, P., Chen, B., Huang, Z., Liu, Z., Zhao, Q., Yi, Y., and Ayers, J. K.: Long-range transport and vertical structure of Asian dust from CALIPSO and surface measurements during PACDEX, Journal of Geophysical Research: Atmospheres, 113, 2008.

Ibusuki, T., and Takeuchi, K.: Sulfur-Dioxide Oxidation by Oxygen Catalyzed by Mixtures of Manganese(Ii) and Iron(Iii) in Aqueous-Solutions at Environmental Reaction Conditions, Atmos. Environ., 21, 1555-1560, Doi 10.1016/0004-6981(87)90317-9, 1987.

Jacob, D. J., and Brasseur, G. P.: Formulations of Radiative, Chemical, and Aerosol Rates, in: Modeling of Atmospheric Chemistry, Cambridge University Press, Cambridge, 205-252, 2017.

Johnson, M. S., Meskhidze, N., Solmon, F., Gasso, S., Chuang, P. Y., Gaiero, D. M., Yantosca, R. M., Wu, S. L., Wang, Y. X., and Carouge, C.: Modeling dust and soluble iron deposition to the South Atlantic Ocean, J Geophys Res-Atmos, 115, Artn D15202

10.1029/2009jd013311, 2010.

Journet, E., Desboeufs, K. V., Caquineau, S., and Colin, J. L.: Mineralogy as a critical factor of dust iron solubility, Geophysical Research Letters, 35, Artn L07805

10.1029/2007gl031589, 2008.

Kong, L., Tang, X., Zhu, J., Wang, Z., Pan, Y., Wu, H., Wu, L., Wu, Q., He, Y., and Tian, S.: Improved inversion of monthly ammonia emissions in China in combination of the Chinese Ammonia Monitoring Network and ensemble Kalman filter, Environ. Sci. Technol., 2019.

Kong, X., Forkel, R., Sokhi, R. S., Suppan, P., Baklanov, A., Gauss, M., Brunner, D., Barò, R., Balzarini, A., Chemel, C., Curci, G., Jiménez-Guerrero, P., Hirtl, M., Honzak, L., Im, U., Pérez, J. L., Pirovano, G., San Jose, R., Schlünzen, K. H., Tsegas, G., Tuccella, P., Werhahn, J., Žabkar, R., and Galmarini, S.: Analysis of meteorology–chemistry interactions during air pollution episodes using online coupled models within AQMEII phase-2, Atmos. Environ., 115, 527-540, 10.1016/j.atmosenv.2014.09.020, 2015.

Lee, Y. N., and Schwartz, S. E.: Precipitation Scavenging, in: Dry Deposition and Resuspension, Elsevier, 453–470, 1983.

Lei, Y., Zhang, Q., He, K., and Streets, D.: Primary anthropogenic aerosol emission trends for China, 1990–2005, Atmospheric Chemistry and Physics, 11, 931-954, 2011.

Li, G. H., Bei, N. F., Cao, J. J., Huang, R. J., Wu, J. R., Feng, T., Wang, Y. C., Liu, S. X., Zhang, Q., Tie, X. X., and Molina, L. T.: A possible pathway for rapid growth of sulfate during haze days in China, Atmos. Chem. Phys., 17, 3301-3316, 10.5194/acp-17-3301-2017, 2017a.

Li, M., Zhang, Q., Streets, D. G., He, K. B., Cheng, Y. F., Emmons, L. K., Huo, H., Kang, S. C., Lu, Z., Shao, M., Su, H., Yu, X., and Zhang, Y.: Mapping Asian anthropogenic emissions of non-methane volatile organic compounds to multiple chemical mechanisms, Atmos. Chem. Phys., 14, 5617-5638, 10.5194/acp-14-5617-2014, 2014.

Li, M., Zhang, Q., Kurokawa, J., Woo, J. H., He, K. B., Lu, Z. F., Ohara, T., Song, Y., Streets, D. G., Carmichael, G. R., Cheng, Y. F., Hong, C. P., Huo, H., Jiang, X. J., Kang, S. C., Liu, F., Su, H., and Zheng, B.: MIX: a mosaic Asian anthropogenic emission inventory under the international collaboration framework of the MICS-Asia and HTAP, Atmos. Chem. Phys., 17, 935-963, 10.5194/acp-17-935-2017, 2017b.

Liu, M. X., Song, Y., Zhou, T., Xu, Z. Y., Yan, C. Q., Zheng, M., Wu, Z. J., Hu, M., Wu, Y. S., and Zhu, T.: Fine particle pH during severe haze episodes in northern China, Geophysical Research Letters, 44, 5213-5221, 10.1002/2017gl073210, 2017.

Liu, Y., Bourgeois, A., Warner, T., Swerdlin, S., and Hacker, J.: Implementation of observation-nudging based FDDA into WRF for supporting ATEC test operations, WRF/MM5 Users′ Workshop June, 2005, 27-30.

Liu, Y. M., Fan, Q., Chen, X. Y., Zhao, J., Ling, Z. H., Hong, Y. Y., Li, W. B., Chen, X. L., Wang, M. J., and Wei, X. L.: Modeling the impact of chlorine emissions from coal combustion and prescribed waste incineration on tropospheric ozone formation in China, Atmos. Chem. Phys., 18, 2709-2724, 10.5194/acp-18-2709-2018, 2018.

Madronich, S.: Photodissociation in the Atmosphere .1. Actinic Flux and the Effects of Ground Reflections and Clouds, J Geophys Res-Atmos, 92, 9740-9752, 10.1029/JD092iD08p09740, 1987.

Makar, P. A., Gong, W., Hogrefe, C., Zhang, Y., Curci, G., Zabkar, R., Milbrandt, J., Im, U., Balzarini, A., Baro, R., Bianconi, R., Cheung, P., Forkel, R., Gravel, S., Hirtl, M., Honzak, L., Hou, A., Jimenez-Guerrero, P., Langer, M., Moran, M. D., Pabla, B., Perez, J.

L., Pirovano, G., San Jose, R., Tuccella, P., Werhahn, J., Zhang, J., and Galmarini, S.: Feedbacks between air pollution and weather, part 2: Effects on chemistry, Atmos. Environ., 115, 499-526, 10.1016/j.atmosenv.2014.10.021, 2015.

Meng, Z. Y., Lin, W. L., Jiang, X. M., Yan, P., Wang, Y., Zhang, Y. M., Jia, X. F., and Yu, X. L.: Characteristics of atmospheric ammonia over Beijing, China, Atmos. Chem. Phys., 11, 6139-6151, 10.5194/acp-11-6139-2011, 2011.

Meskhidze, N., Chameides, W., Nenes, A., and Chen, G.: Iron mobilization in mineral dust: Can anthropogenic SO2 emissions affect ocean productivity?, Geophysical Research Letters, 30, 2003.

Moch, J. M., Dovrou, E., Mickley, L. J., Keutsch, F. N., Cheng, Y., Jacob, D. J., Jiang, J. K., Li, M., Munger, J. W., Qiao, X. H., and Zhang, Q.: Contribution of Hydroxymethane Sulfonate to Ambient Particulate Matter: A Potential Explanation for High Particulate Sulfur During Severe Winter Haze in Beijing, Geophysical Research Letters, 45, 11969-11979, 10.1029/2018gl079309, 2018.

Sandu, A., Verwer, J., Blom, J., Spee, E., Carmichael, G., and Potra, F.: Benchmarking stiff ODE solvers for atmospheric chemistry problems II: Rosenbrock solvers, Atmospheric environment, 31, 3459-3472, 1997.

Sandu, A., and Sander, R.: Technical note: Simulating chemical systems in Fortran90 and Matlab with the Kinetic PreProcessor KPP-2.1, Atmospheric Chemistry and Physics, 6, 187-195, 2006.

Schell, B., Ackermann, I. J., Hass, H., Binkowski, F. S., and Ebel, A.: Modeling the formation of secondary organic aerosol within a comprehensive air quality model system, Journal of Geophysical Research: Atmospheres, 106, 28275-28293, 2001.

Schroth, A. W., Crusius, J., Sholkovitz, E. R., and Bostick, B. C.: Iron solubility driven by speciation in dust sources to the ocean, Nature Geoscience, 2, 337-340, 10.1038/Ngeo501, 2009.

Seinfeld, J. H., and Pandis, S. N.: Atmospheric chemistry and physics: from air pollution to climate change, John Wiley & Sons, 2016.

Shampine, L. F.: Implementation of Rosenbrock methods, ACM Transactions on Mathematical Software (TOMS), 8, 93-113, 1982.

Shao, J. Y., Chen, Q. J., Wang, Y. X., Lu, X., He, P. Z., Sun, Y. L., Shah, V., Martin, R. V., Philip, S., Song, S. J., Zhao, Y., Xie, Z. Q., Zhang, L., and Alexander, B.: Heterogeneous sulfate aerosol formation mechanisms during wintertime Chinese haze events: air quality model assessment using observations of sulfate oxygen isotopes in Beijing, Atmos. Chem. Phys., 19, 6107-6123, 10.5194/acp-19-6107-2019, 2019.

Shi, G., Xu, J., Peng, X., Xiao, Z., Chen, K., Tian, Y., Guan, X., Feng, Y., Yu, H., Nenes, A., and Russell, A. G.: pH of Aerosols in a Polluted Atmosphere: Source Contributions to Highly Acidic Aerosol, Environ Sci Technol, 51, 4289-4296, 10.1021/acs.est.6b05736, 2017.

Shi, Z. B., Krom, M. D., Jickells, T. D., Bonneville, S., Carslaw, K. S., Mihalopoulos, N., Baker, A. R., and Benning, L. G.: Impacts on iron solubility in the mineral dust by processes in the source region and the atmosphere: A review, Aeolian Research, 5, 21-42, 10.1016/j.aeolia.2012.03.001, 2012.

Song, S. J., Gao, M., Xu, W. Q., Shao, J. Y., Shi, G. L., Wang, S. X., Wang, Y. X., Sun, Y. L., and McElroy, M. B.: Fine-particle pH for Beijing winter haze as inferred from different thermodynamic equilibrium models, Atmos. Chem. Phys., 18, 7423-7438, 10.5194/acp-18-7423-2018, 2018.

Song, S. J., Gao, M., Xu, W. Q., Sun, Y. L., Worsnop, D. R., Jayne, J. T., Zhang, Y. Z., Zhu, L., Li, M., Zhou, Z., Cheng, C. L., Lv, Y. B., Wang, Y., Peng, W., Xu, X. B., Lin, N., Wang, Y. X., Wang, S. X., Munger, J. W., Jacob, D. J., and McElroy, M. B.: Possible heterogeneous chemistry of hydroxymethanesulfonate (HMS) in northern China winter haze, Atmos. Chem. Phys., 19, 1357-1371, 10.5194/acp-19-1357-2019, 2019.

Stockwell, W. R., Middleton, P., Chang, J. S., and Tang, X.: The second generation regional acid deposition model chemical mechanism for regional air quality modeling, Journal of Geophysical Research: Atmospheres (1984–2012), 95, 16343-16367, 1990.

Stockwell, W. R., Kirchner, F., Kuhn, M., and Seefeld, S.: A new mechanism for regional atmospheric chemistry modeling, Journal of Geophysical Research: Atmospheres, 102, 25847-25879, 1997.

Sun, Y. L., Jiang, Q., Wang, Z. F., Fu, P. Q., Li, J., Yang, T., and Yin, Y.: Investigation of the sources and evolution processes of severe haze pollution in Beijing in January 2013, J Geophys Res-Atmos, 119, 4380-4398, 10.1002/2014jd021641, 2014.

Takahashi, Y., Higashi, M., Furukawa, T., and Mitsunobu, S.: Change of iron species and iron solubility in Asian dust during the long-range transport from western China to Japan, Atmos. Chem. Phys., 11, 11237-11252, 10.5194/acp-11-11237-2011, 2011.

Tao, W., Liu, J., Ban-Weiss, G., Hauglustaine, D., Zhang, L., Zhang, Q., Cheng, Y., Yu, Y., and Tao, S.: Effects of urban land expansion on the regional meteorology and air quality of eastern China, Atmos. Chem. Phys, 15, 8597-8614, 2015.

Tao, W., Liu, J., Ban-Weiss, G. A., Zhang, L., Zhang, J., Yi, K., and Tao, S.: Potential impacts of urban land expansion on Asian airborne pollutant outflows, Journal of Geophysical Research: Atmospheres, 122, 7646-7663, 2017.

Van Damme, M., Clarisse, L., Whitburn, S., Hadji-Lazaro, J., Hurtmans, D., Clerbaux, C., and Coheur, P. F.: Industrial and agricultural ammonia point sources exposed, Nature, 564, 99-103, 10.1038/s41586-018-0747-1, 2018.

Walcek, C. J., and Taylor, G. R.: A Theoretical Method for Computing Vertical Distributions of Acidity and Sulfate Production within Cumulus Clouds, Journal of the Atmospheric Sciences, 43, 339-355, Doi 10.1175/1520-0469(1986)043<0339:Atmfcv>2.0.Co;2, 1986.

Wang, G., Zhang, R., Gomez, M. E., Yang, L., Levy Zamora, M., Hu, M., Lin, Y., Peng, J., Guo, S., Meng, J., Li, J., Cheng, C., Hu, T., Ren, Y., Wang, Y., Gao, J., Cao, J., An, Z., Zhou, W., Li, G., Wang, J., Tian, P., Marrero-Ortiz, W., Secrest, J., Du, Z., Zheng, J., Shang, D., Zeng, L., Shao, M., Wang, W., Huang, Y., Wang, Y., Zhu, Y., Li, Y., Hu, J., Pan, B., Cai, L., Cheng, Y., Ji, Y., Zhang, F., Rosenfeld, D., Liss, P. S., Duce, R. A., Kolb, C. E., and Molina, M. J.: Persistent sulfate formation from London Fog to Chinese haze, Proc Natl Acad Sci U S A, 113, 13630-13635, 10.1073/pnas.1616540113, 2016.

Wang, H., Zhang, D., Zhang, Y., Zhai, L., Yin, B., Zhou, F., Geng, Y., Pan, J., Luo, J., Gu, B., and Liu, H.: Ammonia emissions from paddy fields are underestimated in China, Environ Pollut, 235, 482-488, 10.1016/j.envpol.2017.12.103, 2018.

Wiedinmyer, C., Akagi, S., Yokelson, R., Emmons, L., Al-Saadi, J., Orlando, J., and Soja, A.: The Fire INventory from NCAR (FINN)—a high resolution global model to estimate the emissions from open burning, Geosci. Model Dev. Discuss, 3, 2439-2476, 2010.

Wu, J., Bei, N., Hu, B., Liu, S., Zhou, M., Wang, Q., Li, X., Liu, L., Feng, T., and Liu, Z.: Is water vapor a key player of the wintertime haze in North China Plain?, Atmos. Chem. Phys., 19, 8721-8739, 2019.

Xu, X., Lin, W., Wang, T., Yan, P., Tang, J., Meng, Z., and Wang, Y.: Long-term trend of surface ozone at a regional background station in eastern China 1991–2006: enhanced variability, Atmos. Chem. Phys., 8, 2595-2607, 2008.

Xue, J., Yu, X., Yuan, Z. B., Griffith, S. M., Lau, A. K. H., Seinfeld, J. H., and Yu, J. Z.: Efficient control of atmospheric sulfate production based on three formation regimes, Nature Geoscience, 12, 977-+, 10.1038/s41561-019-0485-5, 2019.

Zhang, L., Chen, Y. F., Zhao, Y. H., Henze, D. K., Zhu, L. Y., Song, Y., Paulot, F., Liu, X. J., Pan, Y. P., Lin, Y., and Huang, B. X.: Agricultural ammonia emissions in China: reconciling bottom-up and top-down estimates, Atmos. Chem. Phys., 18, 339-355, 10.5194/acp-18-339-2018, 2018a.

Zhang, Q., Streets, D. G., He, K., Wang, Y., Richter, A., Burrows, J. P., Uno, I., Jang, C. J., Chen, D., and Yao, Z.: NOx emission trends for China, 1995–2004: The view from the ground and the view from space, Journal of Geophysical Research: Atmospheres, 112, 2007.

Zhang, Q., Streets, D. G., Carmichael, G. R., He, K. B., Huo, H., Kannari, A., Klimont, Z., Park, I. S., Reddy, S., Fu, J. S., Chen, D., Duan, L., Lei, Y., Wang, L. T., and Yao, Z. L.: Asian emissions in 2006 for the NASA INTEX-B mission, Atmospheric Chemistry and Physics, 9, 5131-5153, 2009.

Zhang, Q., Geng, G., Wang, S., Richter, A., and He, K.: Satellite remote sensing of changes in NO x emissions over China during 1996–2010, Chinese Science Bulletin, 57, 2857-2864, 2012.

Zhang, R., Wang, G., Guo, S., Zamora, M. L., Ying, Q., Lin, Y., Wang, W., Hu, M., and Wang, Y.: Formation of urban fine particulate matter, Chem Rev, 115, 3803-3855, 10.1021/acs.chemrev.5b00067, 2015.

Zhang, R. H., Li, Q., and Zhang, R. N.: Meteorological conditions for the persistent severe fog and haze event over eastern China in January 2013, Sci. China-Earth Sci., 57, 26-35, 10.1007/s11430-013-4774-3, 2014.

Zhang, X. X., Sharratt, B., Liu, L. Y., Wang, Z. F., Pan, X. L., Lei, J. Q., Wu, S. X., Huang, S. Y., Guo, Y. H., Li, J., Tang, X., Yang, T., Tian, Y., Chen, X. S., Hao, J. Q., Zheng, H. T., Yang, Y. Y., and Lyu, Y. L.: East Asian dust storm in May 2017: observations, modelling, and its influence on the Asia-Pacific region, Atmos. Chem. Phys., 18, 8353-8371, 10.5194/acp-18-8353-2018, 2018b.

Zhao, C., Liu, X., Leung, L., Johnson, B., McFarlane, S. A., Gustafson Jr, W., Fast, J. D., and Easter, R.: The spatial distribution of mineral dust and its shortwave radiative forcing over North Africa: modeling sensitivities to dust emissions and aerosol size treatments, Atmos. Chem. Phys., 10, 8821, 2010.

Zhao, C., Chen, S., Leung, L., Qian, Y., Kok, J., Zaveri, R., and Huang, J.: Uncertainty in modeling dust mass balance and radiative forcing from size parameterization, Atmos. Chem. Phys., 13, 10733-10733, 2013.

Zheng, B., Zhang, Q., Zhang, Y., He, K. B., Wang, K., Zheng, G. J., Duan, F. K., Ma, Y. L., and Kimoto, T.: Heterogeneous chemistry: a mechanism missing in current models to explain secondary inorganic aerosol formation during the January 2013 haze episode in North China, Atmos. Chem. Phys., 15, 2031-2049, 10.5194/acp-15-2031-2015, 2015a.

Zheng, G. J., Duan, F. K., Su, H., Ma, Y. L., Cheng, Y., Zheng, B., Zhang, Q., Huang, T., Kimoto, T., Chang, D., Poschl, U., Cheng, Y. F., and He, K. B.: Exploring the severe winter haze in Beijing: the impact of synoptic weather, regional transport and heterogeneous reactions, Atmos. Chem. Phys., 15, 2969-2983, 10.5194/acp-15-2969-2015, 2015b.